Phenotype-genotype relationships in *Xenopus sox9* crispants provide insights into campomelic dysplasia and vertebrate jaw evolution

ツメガエルの *sox9* 変異体群を用いたヒト屈曲肢異形成症と脊椎動物の顎進化の研究

Nusrat Hossain

Graduate School of Integrated Sciences for Life

Hiroshima University

September 2023

Table of Contents

Abstract

Since CRISPR-based genome editing technology works effectively in the diploid frog *Xenopus tropicalis*, a growing number of studies have successfully modeled human genetic diseases in this species. However, most of their targets were limited to non-syndromic diseases that exhibit abnormalities in a small fraction of tissues or organs in the body. This is likely because of the complexity of interpreting the phenotypic variations resulting from somatic mosaic mutations generated in the founder animals (crispants). In this study, I attempted to model the syndromic disease, campomelic dysplasia (CD), by generating *sox9* crispants in *X. tropicalis*. The resulting crispants failed to form neural crest cells at neurula stages and exhibited various combinations of jaw, gill, ear, heart, and gut defects at tadpole stages, recapitulating part of the syndromic phenotype of CD patients. Genotyping of the crispants with a variety of allelic series of mutations suggested that the heart and gut defects depend primarily on frame-shift mutations expected to be null, whereas the jaw, gill, and ear defects could be induced not only by such mutations but also by in-frame deletion mutations expected to delete part of the jawed vertebrate-specific domain from the encoded Sox9 protein. These results demonstrate that *Xenopus* crispants are useful for investigating the phenotype-genotype relationships behind syndromic diseases and examining the tissue-specific role of each functional domain within a single protein, providing novel insights into vertebrate jaw evolution.

1. Introduction:

Genome editing technology with clustered regulatory interspaced short palindromic repeats/CRISPR-associated protein 9 (CRISPR/Cas9) has made a breakthrough in genetic studies through its simplicity and effectiveness (Adli, 2018; Dow, 2015). In vertebrates, crispants (F0 generation mutants) have been generated using various animal models, including mice, zebrafish, and *Xenopus,* by introducing CRISPR reagents into fertilized eggs (Blitz et al., 2013; Hwang et al., 2013; Nakayama et al., 2013; Wang et al., 2013). The resulting mutations generally show mosaicism due to random editing of the target loci in each cell at different stages of embryonic development. Therefore, researchers must breed F1 or F2 generations to obtain uniform germline transmission and non-mosaic (compound heterozygous or homozygous) mutant animals (Aslan et al., 2017; Nakayama et al., 2014). However, such mosaicisms are advantageous in certain cases. These include rapid functional analysis of the genes whose non-mosaic mutations result in early developmental lethality; somatic mosaicism enables the crispants to survive beyond the lethal phase and enables to examine the null phenotype in a specific group of cells (Mehravar et al., 2019; Naert et al., 2021; Zhong et al., 2015). Crispants with mosaic mutations are also useful for studying gene dosage effects, as demonstrated by mouse *Pax6* crispants exhibiting a correlation between the severity of eye defects and the frequency of mutations expected to be null in the allelic series of mutations (Yasue et al., 2017).

Xenopus tropicalis and Xenopus laevis have recently emerged as the time- and cost-effective models for genetic studies, where CRISPR/Cas9 system works quite efficiently (Aslan et al., 2017; Banach et al., 2017; Bharathan & Dickinson, 2019; Bhattacharya et al., 2015; Ezawa et al., 2021; Feehan et al., 2017; Kato et al., 2021; Ledford et al., 2017; Nakayama et al., 2013; Ochi et al., 2017; Tandon et al., 2017; Tanouchi et al., 2022; Tsujioka et al., 2017; Wen et al., 2019; Wyatt et al., 2021). To date, a growing number of studies have successfully modeled human genetic diseases in *Xenopus* crispants, which include defects in the retina, craniofacial structure, kidney, pancreas, left-right axis, limb, and cilium (Delay et al., 2018; Getwan et al., 2021; Naert, 2018; Szenker-Ravi et al., 2018; Tam & Moritz, 2006; Viet et al., 2020; Wyatt et al., 2021). *X. tropicalis* is particularly expected to be suitable for modeling syndromic diseases, since pleiotropic roles of the human genes responsible for

such multi-tissue/organ defects would be conserved in their single orthologs in the diploid genome of *X. tropicalis* but may be partitioned in their duplicated orthologs in the tetraploid genome of *X. laevis* (Hellsten et al., 2010; Session et al., 2016). However, most previous studies in *X. tropicalis* have focused on non-syndromic diseases exhibiting very localized defects or specific aspects of the syndromic disease defects. This is likely because of the complexity of interpreting the phenotypic variations resulting from somatic mosaic mutations generated in the crispants. Thus, it remains elusive whether *X. tropicalis* crispants are indeed useful in modeling such pleiotropic defects and in elucidating phenotype-genotype relationships responsible for the variable appearance of multiple defects in human patients with syndromic diseases.

To address those questions, I chose to study Campomelic Dysplasia (CD; OMIM 114290), a syndromic disease characterized by micrognathia, laryngomalacia, cleft palate, limb deformity, male-to-female sex reversal, hearing impairment, cardiac, renal, lung, and pancreas defects (Houston et al., 1983; Kwok et al., 1995; Mansour et al., 1995; Wagner et al., 1994). The CD is caused by heterozygous mutations in *SOX9* gene that forms a group of *SOXE* ohnologs with *SOX8* and *SOX10* (Bowles et al., 2000; Foster et al., 1994; Wagner et al., 1994). Despite CD being due to single gene mutations, the CD patients show a wide range of phenotypic variations in combining these defects. Micrognathia, laryngomalacia, cleft palate, and limb deformity are common phenotypes of the patients. These phenotypes are often, but not always, accompanied by inner ear abnormalities and/or sex reversal. The defects of other tissues/organs accompany these common phenotypes at a lower frequency (Calvache et al., 2022). Consistent with the human patient phenotype, mouse *Sox9* exhibits expression in the neural crest and derived chondrocytes, genital ridge, otic vesicle, endocardium, metanephric tubules, lung bud, and pancreatic duct epithelium (Ng et al., 1997; Wright et al., 1995). Heterozygous *Sox9* mutant mice mimicked the skeletal abnormalities of CD patients, including micrognathia, laryngomalacia, cleft palate, and limb deformity, but the recapitulation of other tissue/organ defects required the generation of a series of tissue-specific conditional knockout mice, due to perinatal lethality of the heterozygotes (Bi et al., 2001). Therefore, although the multiple

defects in CD have been independently characterized using different sets of mutant mice, knowledge of phenotype-genotype relationships that explain the phenotypic variations in CD is still limited.

This study generated *sox9* crispants in *X. tropicalis* to model CD and reveal the phenotype-genotype relationships underlying their phenotypic variations. The Cas9 duplex guide RNP complexes (dgRNPs) used in this study were designed to introduce mutations in the first exon of *sox9* encoding a jawed vertebrate-specific amino-terminal domain (JAD, Figure 1a). The resulting alleles with frame-shift mutations are expected to be null by failing expression of most part of the Sox9 protein. The alleles with in-frame deletion mutations are expected to express Sox9 proteins lacking part of the JAD. The phenotyping and genotyping analyses in the crispants suggested that the jaw and gill defects, which are orthologous to the human micrognathia and laryngomalacia, and inner ear defects could be induced not only by the frame-shift mutations but also by the in-frame deletion mutations, whereas the defects of other trunk organs depend primarily on the frame-shift mutations. The crispants whose *sox9* alleles mostly encode the JAD-deficient proteins specifically reduced jaw cartilages and formed inwardly concave mouths, suggesting the crucial role of JAD in the evolution of jawed vertebrates.

2. Materials and methods:

2.1 crRNA design and preparation of CRISPR/Cas9 ribonucleoproteins (RNPs)

Two crRNAs (*sox9*-crRNA1, 5'-CAAGAGAACACUUUCCCCAA-3'; *sox9*-crRNA2, 5'-CCGGCUCUGGCUCCGACACG -3') were designed to target the exon 1 of *X. tropicalis sox9* gene with CHOPCHOP (http://chopchop.cbu.uib.no) and IDT web tools (https://sg.idtdna.com). Their target specificities were verified by searching potential off-target sites in *X. tropicalis* genome sequence, allowing one base mismatch (https://gggenome.dbcls.jp/)(Nakayama et al., 2013). Both crRNAs and tracrRNAs were purchased from IDT (IDT Inc., Coralville, USA) and resuspended in Nuclease Free Duplex Buffer (IDT) to obtain a final concentration of 100 μM each. As control experiments, I disrupted *tyrosinase* (*tyr*) locus using a crRNA targeting the same region as reported previously (Nakayama et al., 2013). Afterward, each of the crRNAs was incubated in combination with the tracrRNA at 95°C for 5 minutes in the duplex buffer and then cooled to room temperature. The molecular weight of both crRNA and tracrRNA was used to calculate the final concentration, and the resulting 10 μM dgRNA stock was kept at –25°C for further use. Cas9 protein was commercially obtained from IDT (#1081059) and incubated with the dgRNA at 37°C for 10 minutes in a buffer containing 150 mM KCl and 20 mM Hepes (pH7.5) to prepare duplex guide RNP complexes (dgRNPs). After the incubation, the dgRNPs were kept at room temperature and immediately used for microinjection.

2.2 Microinjections

In vitro fertilization and microinjections were carried out as previously described (Ogino et al., 2006), using eggs and sperms of F1 hybrid animals generated by crossing two inbred *X. tropicalis* strains, *Nigerian H* (*Xtr.NigerianH*^{Huarc}, RRID: HUARC_1002, Xenbase Identifier: XB-LINE-1153) and *Nigerian BH* (*Xtr.NigerianBH*^{Huarc}, RRID: HUARC_1003, Xenbase Identifier: XB-LINE-1163) (Igawa et al., 2015). These animals were provided by Hiroshima University Amphibian Research Center (RRID: SCR_019015) through the National BioResource Project (NBRP) of MEXT. The embryos were staged as previously described (Nieuwkoop & Faber, 1956). Dejellyed eggs were transferred to an injection medium (6% Ficoll, 0.1% BSA in 0.1×MMR) and kept at 20-22ºC. After

fertilization, the dgRNPs containing 100 pg of dgRNA and 1 ng of Cas9 protein were injected into the animal hemisphere of 1-cell stage embryos in a total volume of 2 nl. The injected embryos were kept at 22ºC for 3-4 hours in the injection medium, then transferred into 0.1×MMR without the Ficoll for further development. In all experiments, eGFP mRNA (40 pg) was co-injected with the dgRNPs as a lineage tracer for selecting successfully injected embryos after the gastrulation. The eGFP mRNA was prepared as previously described (Ochi et al., 2017).

2.3 Genotyping

The tadpoles with uniform GFP fluorescence were collected at stages 42–45 and photographed to record their morphological phenotypes. After that, each tadpole was incubated at 95°C for 15 minutes, then digested at 55°C for one overnight in the lysis buffer (100 mM Tris-HCl, pH 8.0; 1 mM EDTA; 0.1% Nonidet P40) along with 10 mg/ml proteinase K treatment. The lysed samples were centrifuged at 20,600 g for 15 min, and the resulting supernatants were harvested as crude genomic DNA samples and stored at –20°C. The 260-bp target regions were amplified from these crude genomic DNA samples using KOD FX Neo DNA polymerase (TOYOBO, Osaka, Japan) with 40 cycles of denaturation at 98°C for 10 seconds, annealing at 66°C for 30 seconds, and extension at 69°C for 60 seconds. The amplified products were cleaned by ExoI/Sap treatment and subjected to Sanger sequencing (Chen et al., 2007). The sequences of PCR primers used are as follows: forward primer, 5’-ATGAAGATGACAGAAGAGCAAGATAAGTGC-3'; reverse primer, 5’-CCATTAACTCTGACTGGCATCGGTACC-3'. The resulting Sangar chromatograms were analyzed with the Inference of CRISPR Edits (ICE) software from Synthego (https://ice.synthego.com/#/) to visualize nucleotide sequences of the composite alleles, and to calculate the rate of each allele and the total indel rate for each crispant (Conant et al., 2022). The ICE analysis has been shown to produce genotyping results consistent with those by next-generation sequencing analysis in previous crispant studies (Liang et al., 2022) (Sieliwonczyk et al., 2023). I used the resulting ICE analysis output for further analysis only when the R-squared value indicating the reliability of the output was greater than the recommended value (0.8) (Conant et al., 2022). Heteroduplex mobility assay (HMA) (Chen et al.,

2012) was performed with those amplicons using a microchip electrophoresis system for DNA/RNA analysis (MCE™ -202 MultiNA; Shimazu, Kyoto, Japan) with the DNA-500 reagent kit.

2.4 *In situ* hybridization, histological analysis, and imaging

Preparation of probes for *Xenopus sox9* (Hayashi et al., 2015)*, snai2* (*slug*, GenBank: BC054144), *sox3* (Zygar et al., 1998), and *atp1a1* (*ATPase Na+/K+ Transporting Subunit Alpha 1*) (McCoy et al., 2008), in situ hybridization with these probes, and breaching of pigments in the stained embryos were performed by following the standard protocol (Sive et al., 2000).

For histological analysis, tadpoles were fixed for one overnight in Bouin's fixative and stored in 70% ethanol (Sive et al., 2000). For whole-mount staining analysis of the cranial cartilages, the skin on the ventral side of the head was removed after the fixed tadpoles were dehydrated through a graded series of ethanol. The resulting tadpoles were subsequently stained with Alcian blue (FUJIFILM Wako Pure Chemical Corporation, Japan). For sectioning analysis, the fixed and dehydrated tadpoles were cleared with xylene, embedded in paraffin blocks, and sectioned into 8 μm thick slices using a microtome. The resulting sections were de-paraffinized, rehydrated, and stained with the Alcian blue and Mayer's hemalum solution (Merck/ EMD, Darmstadt, Germany). The stained samples were mounted in Malinol (MUTO Pure Chemicals, Tokyo, Japan) and covered with cover glass. More than three tadpoles were histologically analyzed for each phenotype category to confirm the reproducibility of internal anatomical features.

Bright-field and fluorescence images of the embryos were taken using a stereoscopic microscope (SMZ1500, Nikon, Tokyo, Japan) with NIS-Elements D Analysis package (4.30.00 64 bit, Nikon).

3. Results

3.1 Generation of *sox9* crispants in *X. tropicalis*

X. tropicalis sox9 gene consists of three exons (Figure 1a; NM_001016853.2, Xtro_10.0, Chr10: 30,591,888–30,597,072). The first exon encodes an amino-terminal domain, a dimerization domain, and part of the HMG domain (Angelozzi & Lefebvre, 2019). The sequence alignment of jawed and jawless vertebrate SoxE-group proteins (Sox8, Sox9, and Sox10 in jawed vertebrates, and SoxE1, SoxE2, and SoxE3 in jawless vertebrates) and the ancestral-type SoxE protein in amphioxus (*Branchiostoma lanceolatum*) shows the unique conservation of the amino-terminal domain in jawed vertebrate Sox9 proteins (jawed vertebrate-specific amino-terminal domain (JAD); Figure 1b). Since *Sox8*, *Sox9,* and *Sox10* were ohnologs generated by whole genome duplications in the ancestral species of vertebrates (Bowles et al., 2000; McCauley & Bronner-Fraser, 2006), the jawed vertebrate *Sox9* appears to have acquired the JAD-encoding sequence after branching off from the jawless vertebrate lineage. This finding is consistent with the previous study that performed comparative misexpression analysis of chick and amphioxus *Sox9* in chick embryos and suggested neofunctionalization of the JAD and carboxyl-terminal domain for the elaboration of neural crest during chordate evolution (Tai et al., 2016).

Targeting a gene of interest with two independent gRNAs and examining phenotypic reproducibility and variation has been established as a standard method for performing F0 embryo assays using *X. tropicalis* (Nakayama et al., 2013). Thus, I designed two guide RNAs, *sox9*-crRNA1 and *sox9*-crRNA2, to target the genomic region encoding a carboxyl-terminal portion of the JAD (Figures 1a, b). The CRISPR/Cas9 mutagenesis with this sox9-crRNA1 or *sox9*-crRNA2 is expected to generate a composite allele that consists of in-frame insertions/deletions and/or frame-shift insertions/deletions, as in previous crispant studies (Mehravar et al., 2019). In the initial experiment, I co-injected eGFP mRNA and the duplex guide RNPs (dgRNPs) prepared from Cas9 protein, tracrRNA, and the *sox9*-crRNA1 or *sox9*-crRNA2 into one-cell stage *X. tropicalis* embryos. I then selected the embryos that gastrulated normally and showed uniform GFP fluorescence at neurula stages (stages 15–17) for further analysis. This is because the uniform GFP fluorescence suggests the

uniform distribution of the co-injected dgRNPs throughout the embryo body, and previous studies have shown that *sox9* knockdown in *Xenopus* using antisense morpholino oligonucleotides (MOs) does not inhibit the gastrulation (Lee et al., 2004; Spokony et al., 2002). I cultured the selected embryos by tadpole stages (stages 42–45), and randomly picked six individuals from the groups injected with *sox9*-crRNA1 and *sox9*-crRNA2, respectively, to assess their mutagenesis efficiency. The genomic DNA was extracted from each of these manipulated and uninjected tadpoles, then used for amplifying the target regions by PCR. In the HMA, most amplicons prepared from tadpoles injected with *sox9*-crRNA1 or *sox9*-crRNA2 migrated slowly as heteroduplex bands compared to the amplicons prepared from uninjected tadpoles, indicating effective disruption of the *sox9* target regions in the injected tadpoles (Figure 2a).

Next, I sequenced the amplicons prepared from *sox9*-crRNA1- or *sox9*-crRNA2-injected tadpoles. Representative examples of their Sanger sequencing chromatograms show overlaid nucleotide sequences in the target regions, indicating the formation of composite alleles with various mutations (Figure 2b). The Sanger chromatograms were subjected to the ICE analysis to examine the composition of mutated alleles in each crispant quantitatively. Representative examples of the ICE analysis outputs show that the targeted alleles contain in-frame deletions, an in-frame insertion, and frame-shift mutations, as expected (Figure 2c). The overall indel rates were more than 75% in those analyzed tadpoles injected with *sox9*-crRNA1 (n = 12) or *sox9*-crRNA2 (n = 11). No significant difference was detected in the indel rates of these two sample groups (Figure 2d).

3.2 Defects in neural crest and other tissue progenitor formation in *sox9* crispants

Since both *sox9*-crRNA1 and *sox9*-crRNA2 were found to be effective in disrupting the target region of *sox9*, I chose to use the *sox9* crispants generated with the *sox9*-crRNA1 to examine whether they fail to form neural crest progenitors as previously shown in *Xenopus sox9* morphants (Lee et al., 2004; Spokony et al., 2002). Whole-mount in situ hybridization analysis showed that the number of embryos normally expressing the neural crest marker *snai2* (*slug*) was significantly decreased in *sox9*-

crRNA1-injected embryos (23/25) compared to their uninjected siblings (1/28) at neural plate stages; the expression was reduced but remained in 60% (15/25) and was not detected in 32% (8/25) of the injected embryos (Figure 3a). I also found that the number of embryos normally expressing the neural plate marker *sox3* was significantly decreased in the injected embryos (19/21) compared to their uninjected siblings (1/23); the expression appeared to be expanded to the neural crest field in 90% (19/21) of the injected embryos (Figure 3b). Such altered expression of *snai2* and *sox3* in *sox9* crispants is consistent with the previously reported gene expression in *sox9* morphants (Lee et al., 2004; Spokony et al., 2002), suggesting that the *sox9*-crRNA1-mediated genome editing specifically disrupted the *sox9* locus.

In addition to *snai2* and *sox3*, I examined the effects of the genome editing on the expression of *sox9*. The number of embryos showing *sox9* expression normally in the neural crest and presumptive otic placode was significantly decreased in *sox9*-crRNA1-injected embryos (56/60) compared to their uninjected siblings (3/71) at the neural plate stages; the expression was reduced but remained in 84% (50/60) and was not detected in 10% (6/60) of the injected embryos (Figure 3c). When examined at tailbud stages, the number of embryos showing normal *sox9* expression in the tissues, including pharyngeal arches, otic vesicle, eye, and brain, was significantly decreased in the injected embryos (11/12) compared to their uninjected siblings (0/15); the expression was reduced but remained in 92% (11/12) of the injected embryos (Figure 3d). The observed reduction of *sox9* expression could be caused by nonsense-mediated decay (NMD) of mRNAs transcribed from the targeted alleles with nonsense or frame-shift mutations, and such NMD could result in down-regulation of the auto-activation mechanism mediated by direct binding of Sox9 protein to the *sox9* promoter (Mead et al., 2013; Parain et al., 2022; Zeng et al., 2002). The remaining *sox9* transcripts detected in the injected embryos may contain mRNAs transcribed from the untargeted wild-type alleles and/or the targeted alleles with missense or in-frame small deletions.

3.3 Syndromic phenotype of *sox9* crispants including jaw, gills, inner ear, heart, gut, and lung defects

The tadpoles injected with *sox9*-crRNA1 exhibited various defects in the jaw, gills, inner ear, heart, and gut at stages 42–45. The jaw and gill defects were manifested as the formation of an inwardly concave mouth (Figure 4a) and a decrease in the gill cavity (Figure 4b, upper panels). Whole-mount Alcian blue-staining of the tadpoles revealed that the jaw and gill defects were associated with hypoplasia of the cranial cartilages. The upper jaw (palatoquadrate) cartilages were deformed, the lower jaw (Meckel's) cartilages were bent inward, and the ceratohyal cartilages were bent inward and reduced. The branchial/gill cartilages were reduced but not so severely deformed compared to the jaw cartilages (Figure 4b, lower panels) (MacKenzie et al., 2022; Sadaghiani & Thiébaud, 1987). Transverse sections of the representative tadpoles stained with Alcian blue and Mayer's hemalum solution showed a decrease in palatoquadrate, ceratohyal, and branchial chondrocytes lining the deformed buccal cavity compared to uninjected tadpoles (Figure 4c). Fifteen percent of the tadpoles injected with *sox9*-crRNA1 exhibited the jaw and gill defects without apparent defects in the inner ear, heart, or gut (n = 73, classified as Category 1 (CA1) in Figures 4h, i). It is noted that I classified phenotypes of the analyzed tadpoles into five categories (CA1–5, Figure 4i) since the tadpoles injected with *sox9*-crRNA1 or *sox9*-crRNA2 showed specific combinatorial patterns of tissue defects. The inner ear defects were identified by the loss or reduction of otoliths (Figure 4d, middle panels). Eleven percent of the *sox9*-crRNA1-injected tadpoles exhibited not only the jaw and gill defects but also such inner ear defects without apparent defects in the heart or gut (classified as Category 2 (CA2) in Figures 4h, i). The heart defects were macroscopically identified by the reduced ventricular size and abnormalities in the blood outflow through the truncus arteriosus (Figure 4e, Supplementary Movie 1). Transverse section analysis revealed that, as in *Sox9* knockout mice, the accumulation of extracellular matrix in their endocardial cushion of the outflow tract (cardiac jelly) was severely reduced in such injected tadpoles compared to uninjected tadpoles (Figure 4f) (Akiyama et al., 2004; Lee & Saint-Jeannet, 2009). Nineteen percent of the *sox9*-crRNA1-injected tadpoles exhibited heart defects in addition to the jaw, gill, and inner ear defects (classified as Category 3 (CA3) in Figures 4h, i). The gut defects were also macroscopically identified by the misorientation and loose coiling

compared to the gut of uninjected tadpoles (Figure 4e). Transverse section analysis revealed that the intestinal lumen was reduced in such injected tadpoles compared to uninjected tadpoles (Figure 4g). Twenty-six percent of the *sox9*-crRNA1-injected tadpoles exhibited gut defects in addition to the jaw, gill, inner ear, and heart defects (classified as Category 4 (CA4) in Figures 4h, i).

In addition to the defects described above, 12% of the tadpoles injected with *sox9*-crRNA1 exhibited a body-bending phenotype (Figure S1, classified as Category 5 (CA5) in Figures 4h, i). However, this phenotype was also induced with similar frequency in tadpoles injected with *tyr*-crRNA (17%, n = 48), suggesting that it is a nonspecific side effect of the microinjection experiment. The remaining tadpoles injected with *tyr*-crRNA exhibited melanin loss instead of the jaw, gill, inner ear, or heart defect as previously reported (83%, n = 48, Figures 4b, d (most right panels), i (bottom graph) (Nakayama et al., 2013). By contrast, the tadpoles injected with *sox9*-crRNA2 exhibited phenotypes at the same categories at similar rates as those injected with *sox9*-crRNA1, demonstrating the specificity and reproducibility of the CA 1, 2, 3, and 4 phenotypes in the genome editing experiments targeting *sox9* (Figure 4i, compare the second and third graphs). The tissue specificity and combinatorial features of these phenotypes are reminiscent of the syndromic phenotype involving dysplasia of the orthologous tissues and organs in human CD patients (Houston et al., 1983; Mansour et al., 2002).

3.4 Phenotype-genotype correlation in *sox9* crispants

The *sox9* crispants generated in this study carried mosaic mutations in the targeted region (Figure 2c). The *sox9* alleles of each crispant contained frame-shift insertions/deletions and/or in-frame insertions/deletions, and their composition varied from one crispant to another. To examine a possible correlation between the phenotypic severity and the allelic composition, I generated a new set of crispants with *sox9*-crRNA1 (n = 51), classified their phenotypes into the five categories (CA 1–5) at the tadpole stages as performed in Figure 4i, and examined their genotypes using the ICE analysis tool. The ICE analysis visualized nucleotide sequences of the composite alleles, and calculated the

rate of each allele and the total indel rate for each crispant (Figure S2). Based on the results of this analysis, I calculated the rates of frame-shift mutations (caused by deletions, insertions, or both deletions and insertions), in-frame deletions without any insertions, and other in-frame mutations caused by insertions or both insertions and deletions. Representative alignments of predicted JAD sequences encoded by the mosaic alleles of CA1 and CA4 tadpoles with the corresponding sequence of wild-type Sox9 protein showed that amino acids ranging from E50 to L60 were deleted by in-frame deletions without any insertions, and amino acids downstream of T52, F53 or P54 were changed to different amino acids or lost by frame-shift mutations (Figure 5a). The alleles with frame-shift mutations are expected to be null, as explained in the introduction. The alleles with in-frame deletions without any insertions are expected to express Sox9 proteins lacking part of the JAD. Predicting the function of other in-frame mutation alleles with insertions or both insertions and deletions is difficult, since the ICE analysis tool cannot distinguish the presence or absence of stop codons in the inserted sequences (see an example in Figure 2c, the in-frame insertion is shown as "NNN"). Thus, I excluded tadpoles carrying such in-frame mutations with insertions for further analysis. I also excluded tadpoles with indel rates of less than 70% to reduce the phenotypic impact of individual differences in genome editing efficiency. Tadpoles with the CA5 phenotype were also excluded, since the body bending phenotype appeared to be induced as a side effect of microinjection experiments, as discussed in Figure 4i.

I plotted indel ratios and frame-shift mutation ratios of the remaining 30 crispants in a graph, and found the formation of two separate groups; the CA 1/2 tadpoles (jaw and gill defects with or without ear defects) formed one, and the CA 3/4 tadpoles (jaw, gill, inner ear, and heart defects with or without gut defects) formed another one (Figure 5b). These two separate groups were also formed when I plotted indel ratios and in-frame deletion ratios of these tadpoles in a graph (Figure 5c). Furthermore, statistical analysis detected significant differences in frame-shift mutation ratios and in-frame deletion ratios between the group of CA 1/2 tadpoles and the group of CA 3/4 tadpoles (Figures 5d, e). The CA 1/2 tadpoles carry frame-shift mutations in 15–37%, and in-frame deletions in 52–77% of their alleles. The CA 3/4 tadpoles have frame-shift mutations in 46–95%, and in-frame deletions in

0–35% of their alleles. Thus, it appears that the heart and gut defects mainly depend on the frame-shift mutations, whereas the jaw, gill, and inner ear defects could be induced not only by the frame-shift mutations but also by the in-frame deletions.

To further examine this possibility, I genotyped the injected tadpoles that exhibited normal morphology. I discovered these tadpoles had frame-shift mutations in 0–30% and in-frame deletions in 2–16% of their alleles (Figures 5b, c, and S3). These tadpoles suggest that the alleles with frame-shift mutations do not induce any apparent defects if their ratio is less than those identified in the CA 3/4 tadpoles and the ratio of in-frame deletions is less than those identified in the CA 1/2 tadpoles, supporting the contribution of in-frame deletions to the jaw, gill, and inner ear phenotype. I found that the maximum in-frame deletion identified in the CA 1/2 tadpoles was 18 bases (Figure S2, blue boxes). The allele carrying this deletion is expected to express *Sox9* protein that lacks only six amino acids from the JAD (Figure 5a, CA1), which again signifies the importance of this targeted region.

4. Discussion

In this study, I generated *sox9* crispants in *X. tropicalis* to examine whether they show syndromic phenotypes similar to those of the human CD patients. The reproducibility and specificity of the genome editing experiments were confirmed by comparing the phenotypes resulting from the independent injections of two different *sox9*-crRNAs that show similar genome editing efficiencies and those resulting from the injection of *tyr*-crRNA. The gene expression analysis in the crispants generated with the *sox9*-crRNA1 showed a decrease in expression of the neural crest marker gene and expanded expression of the neural plate marker gene at the neural plate stages as previously shown in *sox9* morphants, again supporting the specificity of the genome editing. The variations in expression levels of such marker genes and *sox9* appear to reflect the mosaicism of the mutated *sox9* alleles, which was revealed by the genotyping using the ICE analysis tool.

The resulting *sox9* crispants showed specific defects in the jaw, gills, inner ear, heart, and gut at the tadpole stages. The decreases in *sox9*-expressing neural crest cells migrating into the pharyngeal arches account for the jaw and gill defects associated with the reduction and deformity of the upper and lower jaw (palatoquadrate and Meckel's), ceratohyal, and branchial/gill cartilages that are derived from the first, second, and remaining posterior pharyngeal arches, respectively (Sadaghiani & Thiébaud, 1987). The reduction of *sox9* expression in the otic vesicle is consistent with the reduction and/or deformity of otoliths in the ear. These phenotypes are quite similar to the phenotype of *Xenopus sox9* morphants reported by previous studies (Lee et al., 2004; Spokony et al., 2002). Regarding the heart and gut, the expression analysis did not detect *sox9* expression in the primordia of these organs at the tailbud stages. However, previous studies have shown that *sox9* is expressed in the heart endocardium and gut at the later tadpole stages in *Xenopus* (Lee & Saint-Jeannet, 2003, 2009). Thus, the reduction of *sox9* activity in the heart and gut may directly account for the dysplasia of these organs in the crispants. No previous studies have reported such heart or gut defects in *Xenopus sox9* morphants, which may be due to the inefficacy of the morpholino injections in blocking the *sox9* function for heart and gut development.

The phenotype of *sox9* crispants recapitulated part of the phenotypes of human CD patients and *Sox9* mutant mice (Bi et al., 2001; Pritchett et al., 2011). The jaw and gill defects in the crispants are orthologous to the micrognathia and laryngomalacia in the human patients and mutant mice. The inner ear defects in the crispants, including the deformity or loss of otolith, may correspond to the inner ear anomalies in the human patients and in the mice whose *Sox9* was conditionally disrupted in the otic ectoderm (Barrionuevo et al., 2008; Saint-Germain et al., 2004). The heart defects in the crispants, including ventricle dysplasia, reduced cardiac jelly in the outflow tract, and abnormal blood outflow, appear to be related to cardiac anomalies with heart failure in the human patients and *Sox9*-null mice (Akiyama et al., 2004; Houston et al., 1983). The gut defects in the crispants, including the intestinal lumen dysplasia, may be related to the intestinal crypt hyperplasia in the mice whose *Sox9* was conditionally disrupted in the intestinal epithelium (Bastide et al., 2007). In addition to the defects described above, I revealed pronephric defects in tailbud-stage crispants by in situ hybridization analysis of a pronephric marker gene, *atp1a1*, expression (Figure S4, 75% (12/16)), though it was difficult to score morphological defects in the pronephros of tadpole-stage crispants macroscopically. The observed defects in proximal and/or distal tubule formation may also be related to the kidney anomalies of human CD patients, including renal hypoplasia, and the role of mouse *Sox9* in the nephric epithelial branching (Reginensi et al., 2011). However, I was not able to examine whether the *sox9* crispants could recapitulate other features of CD patients, such as the limb skeletal anomaly, male-to-female sex reversal, and lung and pancreas dysplasia or not. This is because the crispant tadpoles were hard to survive until they formed visually detectable limbs, genital structures, and lungs (Nieuwkoop & Faber, 1956; Rankin et al., 2015). Possible defects in the pancreas were also macroscopically undetectable by the examined stages. Investigation of these potential defects would require further elaborate analysis, which is beyond the scope of this study, whose aim was to explore the availability of *X. tropicalis* crispants for modeling the syndromic disease and possible phenotype-genotype relationships behind its phenotypic variations.

The *sox9* crispants exhibited the jaw, gills, inner ear, heart, and gut defects with their specific combinations classified into CA 1 to 4. The observed combinatorial patterns appear analogous to

those caused by the heterozygous mutations in human CD patients. Micrognathia and laryngomalacia are common phenotypes of the patients and are often but not always, accompanied by inner ear abnormalities (Calvache et al., 2022). Cardiac anomalies accompany these common phenotypes at a lower frequency, and intestinal anomalies accompany them as rare cases (Houston et al., 1983). Thus, it may be possible to study part of the mechanisms that produce the combinatorial patterns of CD-related defects in the crispants, without reproducing heterozygous mutations close to those of the human patients.

The CA 1/2 phenotype (jaw and gill defects with or without inner ear defects), which could be induced by the JAD in-frame deletions, is especially interesting in relation to the human patients who exhibit micrognathia, laryngomalacia, and hearing impairment but no apparent anomalies in the heart or intestine. It has been shown that one of these patients carries a missense mutation (H65Y) in the dimerization domain (DIM)-encoding sequence of *SOX9*, and the resulting mutant protein possesses weaker DNA-binding activity compared to the wild-type protein (McDowall et al., 1999). Other patients also carry missense mutations (A76E) in the DIM-encoding sequence, and the resulting mutant protein fails to activate transcription from chondrocyte-specific enhancers of *Col11a2* and *Col9a2* genes but activates transcription from a testis-specific enhancer of *Sf1* (Bernard et al., 2003; Sock et al., 2003; Takenouchi et al., 2014). Given the close location of the JAD in-frame deletions (around E50 to L60) to these human CD mutations (H65Y and A76E) and the similarity between the DIM missense mutation phenotype and the CA 1/2 phenotype, the JAD in-frame deletions possibly affected the target gene specificity of the encoded Sox9 protein by modulating its dimerization and DNA-binding activity. The in-frame deletions may also have inhibited SUMOylation of the amino acid close to the deleted regions (K61, Figure 5a), though the functional importance of this potential SUMOylation site has remained unclear (Taylor & LaBonne, 2005). The CA 1 tadpoles with the inwardly concave mouth are reminiscent of the lamprey, a jawless vertebrate that expresses a JAD region-deficient ortholog (*SoxE3*) of *Sox9* in the first pharyngeal arch, suggesting the importance of JAD in the evolution of jawed vertebrates (McCauley & Bronner-Fraser, 2006). Future studies may

reveal close relationships between the cranial morphology of the ancestral-type vertebrate and jaw defects caused by the JAD mutations.

The CA 3/4 phenotype (jaw, gill, ear, and heart defects with or without gut defects) showed a critical dependence on the frame-shift mutations in the JAD-encoding sequence that are expected to be null. This finding is consistent with the studies that identified nonsense mutations in the JAD-encoding sequence of *SOX9* of human CD patients with severe pleiotropic defects, including micrognathia and cardiac anomalies (Calvache et al., 2022). Thus, the phenotype-genotype correlation analysis and the previous studies of human CD patients suggest that JAD-specific and DIM-specific functions of Sox9 are dispensable for the heart and gut formation but not for the cranial cartilage and inner ear formation. Regarding the possible relationship between the severity of a particular phenotype and the mutation type, the CA 3/4 tadpoles may have exhibited more severe deformities in the jaw and gill cartilages than the CA 1/2 tadpoles. However, I could not detect such quantitative differences due to phenotypic variations of the crispants in this study.

Since mice carrying heterozygous null mutations in *Sox9* exhibit severe respiratory failure and die shortly after birth, further analyses of the cardiac and intestinal defects require a series of tissue-specific conditional knockout mice (Akiyama et al., 2002, 2004; Bastide et al., 2007). By contrast, *Xenopus sox9* crispants survived until the swimming tadpole stages and exhibited the cardiac and intestinal defects together with the jaw, gill, and ear defects. This difference between mice and *Xenopus* can be partially attributed to the use of gills for gas exchange in the tadpoles (Rose & James, 2013). In this study, such advantage of *Xenopus* for studying multiple organ/tissue defects and the mosaicism in crispant mutations provided us the opportunity to examine the phenotype-genotype relationships that have remained unclear in previous CD studies (Meyer et al., 1997). Moreover, the jaw dysplasia phenotype of the crispants, which appeared to be caused by the partial truncation of JAD, highlights the use of crispants for investigating tissue-specific roles for each functional domain included in a single protein, and provides a novel insight into the jaw evolution.

References

Adli, M. (2018). The CRISPR tool kit for genome editing and beyond. *Nature Communications*, *9*(1), 1911. https://doi.org/10.1038/s41467-018-04252-2

Akiyama, H., Chaboissier, M. C., Martin, J. F., Schedl, A., & De Crombrugghe, B. (2002). The transcription factor *Sox9* has essential roles in successive steps of the chondrocyte differentiation pathway and is required for expression of *Sox5* and *Sox6*. *Genes and Development*, *16*(21), 2813–2828. https://doi.org/10.1101/gad.1017802

Akiyama, H., Chaboissier, M.-C., Behringer, R. R., Rowitch, D. H., Schedl, A., Epstein, J. A., & de Crombrugghe, B. (2004). Essential role of *Sox9* in the pathway that controls formation of cardiac valves and septa. *Proceedings of the National Academy of Sciences*, *101*(17), 6502–6507. https://doi.org/10.1073/pnas.0401711101

Angelozzi, M., & Lefebvre, V. (2019). SOXopathies: Growing Family of Developmental Disorders Due to SOX Mutations. *Trends in Genetics*, *35*(9), 658–671. https://doi.org/10.1016/j.tig.2019.06.003

Aslan, Y., Tadjuidje, E., Zorn, A. M., & Cha, S.-W. (2017). High efficiency non-mosaic CRISPR mediated knock-in and mutations in F0 *Xenopus*. *Development*, *144*(15), 2852–2858. https://doi.org/10.1242/dev.152967

Banach, M., Edholm, E. S., & Robert, J. (2017). Exploring the functions of nonclassical MHC class Ib genes in *Xenopus laevi*s by the CRISPR/Cas9 system. *Developmental Biology*, *426*(2), 261–269. https://doi.org/10.1016/j.ydbio.2016.05.023

Barrionuevo, F., Naumann, A., Bagheri-Fam, S., Speth, V., Taketo, M. M., Scherer, G., & Neubüser, A. (2008). *Sox9* is required for invagination of the otic placode in mice. *Developmental Biology*, *317*(1), 213–224. https://doi.org/10.1016/j.ydbio.2008.02.011

Bastide, P., Darido, C., Pannequin, J., Kist, R., Robine, S., Marty-Double, C., Bibeau, F., Scherer, G., Joubert, D., Hollande, F., Blache, P., & Jay, P. (2007). *Sox9* regulates cell proliferation and is required for Paneth cell differentiation in the intestinal epithelium. *Journal of Cell Biology*, *178*(4), 635–648. https://doi.org/10.1083/jcb.200704152

Bernard, P., Tang, P., Liu, S., Dewing, P., Harley, V. R., & Vilain, E. (2003). Dimerization of *SOX9* is required for chondrogenesis, but not for sex determination. *Human Molecular Genetics*, *12*(14), 1755–1765. https://doi.org/10.1093/hmg/ddg182

Bharathan, N. K., & Dickinson, A. J. G. (2019). Desmoplakin is required for epidermal integrity and morphogenesis in the *Xenopus laevis* embryo. *Developmental Biology*, *450*(2), 115–131. https://doi.org/10.1016/j.ydbio.2019.03.010

Bhattacharya, D., Marfo, C. A., Li, D., Lane, M., & Khokha, M. K. (2015). CRISPR/Cas9: An inexpensive, efficient loss of function tool to screen human disease genes in *Xenopus*. *Developmental Biology*, *408*(2), 196–204. https://doi.org/10.1016/j.ydbio.2015.11.003

Bi, W., Huang, W., Whitworth, D. J., Deng, M., Zhang, Z., Behringer, R. R., & De Crombrugghe, B. (2001). Haploinsufficiency of *Sox9* results in defective cartilage primordia and premature skeletal mineralization. *Proc Natl Acad Sci U S A*, *98*(12), 6698-7–3. https://doi.org/10.1073/pnas.111092198

Blitz, I. L., Biesinger, J., Xie, X., & Cho, K. W. (2013). Biallelic genome modification in F(0) *Xenopus tropicalis* embryos using the CRISPR/Cas system. *Genesis*, 51(12), 827–834. https://doi.org/10.1002/dvg.22719

Bowles, J., Schepers, G., & Koopman, P. (2000). Phylogeny of the SOX Family of Developmental Transcription Factors Based on Sequence and Structural Indicators. *Developmental Biology*, *227*(2), 239–255. https://doi.org/10.1006/dbio.2000.9883

Calvache, C. A., Vásquez, E. C., Romero, V. I., Hosomichi, K., & Pozo, J. C. (2022). Novel SRY-box transcription factor 9 variant in campomelic dysplasia and the location of missense and nonsense variants along the protein domains: A case report. *Frontiers in Pediatrics*, *10,975947*. https://doi.org/10.3389/fped.2022.975947

Chen, J., Zhang, X., Wang, T., Li, Z., Guan, G., & Hong, Y. (2012). Efficient Detection, Quantification and Enrichment of Subtle Allelic Alterations. *DNA Research*, *19*(5), 423–433. https://doi.org/10.1093/dnares/dss023

Chen, X. S., Rozhdestvensky, T. S., Collins, L. J., Schmitz, J., & Penny, D. (2007). Combined experimental and computational approach to identify non-protein-coding RNAs in the deep-

branching eukaryote Giardia intestinalis. *Nucleic Acids Research*, *35*(14), 4619–4628. https://doi.org/10.1093/nar/gkm474

Conant, D., Hsiau, T., Rossi, N., Oki, J., Maures, T., Waite, K., Yang, J., Joshi, S., Kelso, R., Holden, K., Enzmann, B. L., & Stoner, R. (2022). Inference of CRISPR Edits from Sanger Trace Data. *The CRISPR Journal*, *5*(1), 123–130. https://doi.org/10.1089/crispr.2021.0113

Delay, B. D., Corkins, M. E., Hanania, H. L., Salanga, M., Deng, J. M., Sudou, N., Taira, M., Horb, M. E., & Miller, R. K. (2018). Tissue-specific gene inactivation in *Xenopus laevis*: Knockout of *lhx1* in the kidney with CRISPR/Cas9. *Genetics*, *208*(2), 673–686. https://doi.org/10.1534/genetics.117.300468

Dow, L. E. (2015). Modeling Disease In Vivo With CRISPR/Cas9. *Trends in Molecular Medicine*, *21*(10), 609–621. https://doi.org/10.1016/j.molmed.2015.07.006

Ezawa, M., Kouno, F., Kubo, H., Sakuma, T., Yamamoto, T., & Kinoshita, T. (2021). Pou5f3.3 is involved in establishment and maintenance of hematopoietic cells during *Xenopus* development. *Tissue and Cell*, *72*. https://doi.org/10.1016/j.tice.2021.101531

Feehan, J. M., Chiu, C. N., Stanar, P., Tam, B. M., Ahmed, S. N., & Moritz, O. L. (2017). Modeling Dominant and Recessive Forms of Retinitis Pigmentosa by Editing Three Rhodopsin-Encoding Genes in Xenopus Laevis Using Crispr/Cas9. *Scientific Reports*, *7*(1). https://doi.org/10.1038/s41598-017-07153-4

Foster, J. W., Dominguez-Steglich, M. A., Guioli, S., Kwok, C., Weller, P. A., Stevanovic, M., Weissenbacht, J., Mansour, S., Young, L. D., Goodfellow, P. N., David Brook, J., & Schafer, A. J. (1994). Campomelic dysplasia and autosomal sex reversal caused by mutations in an SRY-related gene. *Nature*, *372*, 525–530. https://doi.org/https://doi.org/10.1038/372525a0

Getwan, M., Hoppmann, A., Schlosser, P., Grand, K., Song, W., Diehl, R., Schroda, S., Heeg, F., Deutsch, K., Hildebrandt, F., Lausch, E., Köttgen, A., & Lienkamp, S. S. (2021). *Ttc30a* affects tubulin modifications in a model for ciliary chondrodysplasia with polycystic kidney disease. *Proc Natl Acad Sci U S A*, *118*(39),e2106770118. https://doi.org/10.1073/pnas.2106770118

Hayashi, S., Kobayashi, T., Yano, T., Kamiyama, N., Egawa, S., Seki, R., Takizawa, K., Okabe, M., Yokoyama, H., & Tamura, K. (2015). Evidence for an amphibian sixth digit. *Zoological Letters*, *1*(1),17. https://doi.org/10.1186/s40851-015-0019-y

Hellsten, U., Harland, R. M., Gilchrist, M. J., Hendrix, D., Jurka, J., Kapitonov, V., Ovcharenko, I., Putnam, N. H., Shu, S., Taher, L., Blitz, I. L., Blumberg, B., Dichmann, D. S., Dubchak, L., Amaya, E., Detter, J. C., Fletcher, R., Gerhard, D. S., Goodstein, D., … Rokhsar, D. S. (2010). The genome of the western clawed frog *Xenopus tropicalis*. *Science*, *328*(5978), 633–636. https://doi.org/10.1126/science.1183670

Houston, C. S., Opitz, J. M., Spranger, J. W., Macpherson, R. I., Reed, M. H., Gilbert, E. F., Herrmann, J., & Schinzel, A. (1983). The campomelic syndrome: Review, report of 17 cases, and follow-up on the currently 17-year-old boy first reported by Maroteaux et al in 1971. *American Journal of Medical Genetics, 15*(1), 3–28. https://doi.org/10.1002/ajmg.1320150103

Hwang, W. Y., Fu, Y., Reyon, D., Maeder, M. L., Tsai, S. Q., Sander, J. D., Peterson, R. T., Yeh, J. R., & Joung, J. K. (2013). Efficient genome editing in zebrafish using a CRISPR-Cas system. *Nature biotechnology*, 31(3), 227–229. https://doi.org/10.1038/nbt.2501

Igawa, T., Watanabe, A., Suzuki, A., Kashiwagi, A., Kashiwagi, K., Noble, A., Guille, M., Simpson, D. E., Horb, M. E., Fujii, T., & Sumida, M. (2015). Inbreeding ratio and genetic relationships among strains of the western clawed frog, *Xenopus tropicalis*. *PLoS ONE*, *10*(7). https://doi.org/10.1371/journal.pone.0133963

Kato, S., Fukazawa, T., & Kubo, T. (2021). Low-temperature incubation improves both knock-in and knock-down efficiencies by the CRISPR/Cas9 system in *Xenopus laevis* as revealed by quantitative analysis. *Biochemical and Biophysical Research Communications*, *543*, 50–55. https://doi.org/10.1016/j.bbrc.2020.11.038

Kwok, C., Weller, P. A., Guioli, S., Foster, J. W., Mansour, S., Zuffardi, O., Punnett, H. H., Dominguez-Steglich, M. A., Brook, J. D., & Young, I. D. (1995). Mutations in *SOX9*, the gene responsible for Campomelic dysplasia and autosomal sex reversal. *American Journal of Human Genetics*, *57*(5), 1028–1036. http://www.ncbi.nlm.nih.gov/pubmed/7485151

Ledford, K. L., Martinez-De Luna, R. I., Theisen, M. A., Rawlins, K. D., Viczian, A. S., & Zuber, M. E. (2017). Distinct cis-acting regions control *six6* expression during eye field and optic cup stages of eye formation. *Developmental Biology*, *426*(2), 418–428. https://doi.org/10.1016/j.ydbio.2017.04.003

Lee, Y.-H., & Saint-Jeannet, J.-P. (2009). Characterization of molecular markers to assess cardiac cushions formation in *Xenopus*. *Developmental Dynamics*, *238*(12), 3257–3265. https://doi.org/10.1002/dvdy.22148

Lee, Y.-H., & Saint-Jeannet, J.-P. (2003). *Sox9*, a novel pancreatic marker in *Xenopus*. *The International Journal of Developmental Biology*, *47*(6), 459–462. http://www.ncbi.nlm.nih.gov/pubmed/14584783

Lee, Y.-H., Aoki, Y., Hong, C.-S., Saint-Germain, N., Credidio, C., & Saint-Jeannet, J.-P. (2004). Early requirement of the transcriptional activator *Sox9* for neural crest specification in *Xenopus*. *Developmental Biology*, *275*(1), 93–103. https://doi.org/10.1016/j.ydbio.2004.07.036

Liang, F., Zhang, Y., Li, L., Yang, Y., Fei, J.-F., Liu, Y., & Qin, W. (2022). SpG and SpRY variants expand the CRISPR toolbox for genome editing in zebrafish. *Nature Communications*, *13*(1), 3421. https://doi.org/10.1038/s41467-022-31034-8

MacKenzie, E. M., Atkins, J. B., Korneisel, D. E., Cantelon, A. S., McKinnell, I. W., & Maddin, H. C. (2022). Normal development in *Xenopus laevis*: A complementary staging table for the skull based on cartilage and bone. *Developmental Dynamics*, *251*(8), 1340–1356. https://doi.org/10.1002/dvdy.465

Mansour, S., Hall, C. M., Pembrey, M. E., & Young, I. D. (1995). A clinical and genetic study of campomelic dysplasia. *Journal of Medical Genetics*, *32*(6), 415–420. https://doi.org/10.1136/jmg.32.6.415

Mansour, S., Offiah, A. C., McDowall, S., Sim, P., Tolmie, J., & Hall, C. (2002). The phenotype of survivors of campomelic dysplasia. *Journal of Medical Genetics*, *39*(8), 597–602. https://doi.org/10.1136/jmg.39.8.597

McCauley, D. W., & Bronner-Fraser, M. (2006). Importance of SoxE in neural crest development and the evolution of the pharynx. *Nature*, *441*(7094), 750–752. https://doi.org/10.1038/nature04691

McCoy, K. E., Zhou, X., & Vize, P. D. (2008). Collectrin/tmem27 is expressed at high levels in all segments of the developing *Xenopus* pronephric nephron and in the Wolffian duct. *Gene Expression Patterns*, *8*(4), 271–274. https://doi.org/10.1016/j.gep.2007.12.002

McDowall, S., Argentaro, A., Ranganathan, S., Weller, P., Mertin, S., Mansour, S., Tolmie, J., & Harley, V. (1999). Functional and Structural Studies of Wild Type *SOX9* and Mutations Causing Campomelic Dysplasia. *Journal of Biological Chemistry*, *274*(34), 24023–24030. https://doi.org/10.1074/jbc.274.34.24023

Mead, T. J., Wang, Q., Bhattaram, P., Dy, P., Afelik, S., Jensen, J., & Lefebvre, V. (2013). A far-upstream (-70 kb) enhancer mediates *Sox9* auto-regulation in somatic tissues during development and adult regeneration. *Nucleic Acids Research*, *41*(8), 4459–4469. https://doi.org/10.1093/nar/gkt140

Mehravar, M., Shirazi, A., Nazari, M., & Banan, M. (2019). Mosaicism in CRISPR/Cas9-mediated genome editing. *Developmental Biology*, *445*(2), 156–162. https://doi.org/10.1016/j.ydbio.2018.10.008

Meyer, J., Südbeck, P., Held, M., Wagner, T., Schmitz, M. L., Bricarelli, F. D., Eggermont, E., Friedrich, U., Haas, O. A., Kobelt, A., Leroy, J. G., Van Maldergem, L., Michel, E., Mitulla, B., Pfeiffer, R. A., Schinzel, A., Schmidt, H., & Scherer, G. (1997). Mutational analysis of the SOX9 gene in campomelic dysplasia and autosomal sex reversal: lack of genotype/phenotype correlations. *Human molecular genetics*, *6*(1), 91–98. https://doi.org/10.1093/hmg/6.1.91

Naert, T., Tulkens, D., Van Nieuwenhuysen, T., Przybyl, J., Demuynck, S., van de Rijn, M., Al-Jazrawe, M., Alman, B. A., Coucke, P. J., De Leeneer, K., Vanhove, C., Savvides, S. N., Creytens, D., & Vleminckx, K. (2021). CRISPR-SID: Identifying EZH2 as a druggable target for desmoid tumors via in vivo dependency mapping. *Proceedings of the National Academy of Sciences*, *118*(47),e2115116118. https://doi.org/10.1073/pnas.2115116118

Naert, T., & Vleminckx, K. (2018). CRISPR/Cas9 disease models in zebrafish and *Xenopus*: The genetic renaissance of fish and frogs. *Drug Discovery Today: Technologies*, *28*, 41–52. https://doi.org/10.1016/j.ddtec.2018.07.001

Nakayama, T., Fish, M. B., Fisher, M., Oomen-Hajagos, J., Thomsen, G. H., & Grainger, R. M. (2013). Simple and efficient CRISPR/Cas9-mediated targeted mutagenesis in *Xenopus tropicalis*. *Genesis*, *51*(12), 835–843. https://doi.org/10.1002/dvg.22720

Nakayama, T., Blitz, I. L., Fish, M. B., Odeleye, A. O., Manohar, S., Cho, K. W., & Grainger, R. M. (2014). Cas9-based genome editing in *Xenopus tropicalis*. *Methods in enzymology*, 546, 355–375. https://doi.org/10.1016/B978-0-12-801185-0.00017-9

Ng, L.-J., Wheatley, S., Muscat, G. E. O., Conway-Campbell, J., Bowles, J., Wright, E., Bell, D. M., Tam, P. P. L., Cheah, K. S. E., & Koopman, P. (1997). *SOX9* Binds DNA, Activates Transcription, and Coexpresses with Type II Collagen during Chondrogenesis in the Mouse. *Developmental Biology*, *183*(1), 108–121. https://doi.org/10.1006/dbio.1996.8487

Nieuwkoop, P. D., & Faber, J. (1956). Normal Table of *Xenopus laevis* (Daudin). North Holland Publishing Co.

Ochi, H., Kawaguchi, A., Tanouchi, M., Suzuki, N., Kumada, T., Iwata, Y., & Ogino, H. (2017). Co-accumulation of cis-regulatory and coding mutations during the pseudogenization of the *Xenopus laevis* homoeologs *six6.L* and *six6.S*. *Developmental Biology*, *427*(1), 84–92. https://doi.org/10.1016/j.ydbio.2017.05.004

Ogino, H., McConnell, W. B., & Grainger, R. M. (2006). High-throughput transgenesis in *Xenopus* using I-SceI meganuclease. *Nature Protocols*, *1*(4), 1703–1710. https://doi.org/10.1038/nprot.2006.208

Parain, K., Lourdel, S., Donval, A., Chesneau, A., Borday, C., Bronchain, O., Locker, M., & Perron, M. (2022). CRISPR/Cas9-Mediated Models of Retinitis Pigmentosa Reveal Differential Proliferative Response of Müller Cells between *Xenopus laevis* and *Xenopus tropicalis. Cells*, *11*(5),807. https://doi.org/10.3390/cells11050807

Pritchett, J., Athwal, V., Roberts, N., Hanley, N. A., & Hanley, K. P. (2011). Understanding the role of *SOX9* in acquired diseases: lessons from development. *Trends in Molecular Medicine*, *17*(3), 166–174. https://doi.org/10.1016/j.molmed.2010.12.001

Rankin, S. A., Thi Tran, H., Wlizla, M., Mancini, P., Shifley, E. T., Bloor, S. D., Han, L., Vleminckx, K., Wert, S. E., & Zorn, A. M. (2015). A Molecular atlas of *Xenopus* respiratory system development. *Developmental Dynamics*, *244*(1), 69–85. https://doi.org/10.1002/dvdy.24180

Reginensi, A., Clarkson, M., Neirijnck, Y., Lu, B., Ohyama, T., Groves, A. K., Sock, E., Wegner, M., Costantini, F., Chaboissier, M. C., & Schedl, A. (2011). *SOX9* controls epithelial branching by activating RET effector genes during kidney development. *Human Molecular Genetics*, *20*(6), 1143–1153. https://doi.org/10.1093/hmg/ddq558

Rose, C. S., & James, B. (2013). Plasticity of lung development in the amphibian, *Xenopus laevis*. *Biology Open*, *2*(12), 1324–1335. https://doi.org/10.1242/bio.20133772

Sadaghiani, B., & Thiébaud, C. H. (1987). Neural crest development in the *Xenopus laevis* embryo, studied by interspecific transplantation and scanning electron microscopy. *Developmental Biology*, *124*(1), 91–110. https://doi.org/10.1016/0012-1606(87)90463-5

Saint-Germain, N., Lee, Y.-H., Zhang, Y., Sargent, T. D., & Saint-Jeannet, J.-P. (2004). Specification of the otic placode depends on *Sox9* function in *Xenopus*. *Development*, *131*(8), 1755–1763. https://doi.org/10.1242/dev.01066

Session, A. M., Uno, Y., Kwon, T., Chapman, J. A., Toyoda, A., Takahashi, S., Fukui, A., Hikosaka, A., Suzuki, A., Kondo, M., van Heeringen, S. J., Quigley, I., Heinz, S., Ogino, H., Ochi, H., Hellsten, U., Lyons, J. B., Simakov, O., Putnam, N., … Rokhsar, D. S. (2016). Genome evolution in the allotetraploid frog *Xenopus laevis*. *Nature*, *538*(7625), 336–343. https://doi.org/10.1038/nature19840

Sieliwonczyk, E., Vandendriessche, B., Claes, C., Mayeur, E., Alaerts, M., Holmgren, P., Canter Cremers, T., Snyders, D., Loeys, B., & Schepers, D. (2023). Improved selection of zebrafish CRISPR editing by early next-generation sequencing based genotyping. *Scientific Reports*, *13*(1), 1491. https://doi.org/10.1038/s41598-023-27503-9

Sive, H., Grainger, R., & Harland, R. (2000). *Early Development of Xenopus Laevis: A Laboratory Manual* . Cold Spring Harbor Laboratory Press, New York (2000).

Sock, E., Pagon, R. A., Keymolen, K., Lissens, W., Wegner, M., & Scherer, G. (2003). Loss of DNA-dependent dimerization of the transcription factor *SOX9* as a cause for campomelic dysplasia. *Human Molecular Genetics*, *12*(12), 1439–1447. https://doi.org/10.1093/hmg/ddg158

Spokony, R. F., Aoki, Y., Saint-Germain, N., Magner-Fink, E., & Saint-Jeannet, J.-P. (2002). The transcription factor *Sox9* is required for cranial neural crest development in *Xenopus*. *Development*, *129*(2), 421–432. https://doi.org/10.1242/dev.129.2.421

Szenker-Ravi, E., Altunoglu, U., Leushacke, M., Bosso-Lefèvre, C., Khatoo, M., Thi Tran, H., Naert, T., Noelanders, R., Hajamohideen, A., Beneteau, C., De Sousa, S. B., Karaman, B., Latypova, X., Başaran, S., Yücel, E. B., Tan, T. T., Vlaminck, L., Nayak, S. S., Shukla, A., … Reversade, B. (2018). RSPO2 inhibition of RNF43 and ZNRF3 governs limb development independently of LGR4/5/6. *Nature*, *557*(7706), 564–569. https://doi.org/10.1038/s41586-018-0118-y

Tai, A., Cheung, M., Huang, Y.-H., Jauch, R., Bronner, M. E., & Cheah, K. S. E. (2016). SOXE neofunctionalization and elaboration of the neural crest during chordate evolution. *Scientific Reports*, *6*(1), 34964. https://doi.org/10.1038/srep34964

Takenouchi, T., Matsuzaki, Y., Yamamoto, K., Kosaki, K., Torii, C., Takahashi, T., & Kosaki, K. (2014). *SOX9* dimerization domain mutation mimicking type 2 collagen disorder phenotype. *European Journal of Medical Genetics*, *57*(6), 298–301. https://doi.org/10.1016/j.ejmg.2014.03.012

Tam, B. M., & Moritz, O. L. (2006). Characterization of Rhodopsin P23H-Induced Retinal Degeneration in a *Xenopus laevis* Model of Retinitis Pigmentosa. *Investigative Opthalmology & Visual Science*, *47*(8), 3234. https://doi.org/10.1167/iovs.06-0213

Tandon, P., Conlon, F., Furlow, J. D., & Horb, M. E. (2017). Expanding the genetic toolkit in *Xenopus*: Approaches and opportunities for human disease modeling. *Developmental Biology*, *426*(2), 325–335. https://doi.org/10.1016/j.ydbio.2016.04.009

Tanouchi, M., Igawa, T., Suzuki, N., Suzuki, M., Hossain, N., Ochi, H., & Ogino, H. (2022). Optimization of CRISPR/Cas9 -mediated gene disruption in *Xenopus laevis* using a phenotypic image analysis technique. *Development, Growth & Differentiation*. https://doi.org/10.1111/dgd.12778

Taylor, K. M., & LaBonne, C. (2005). SoxE Factors Function Equivalently during Neural Crest and Inner Ear Development and Their Activity Is Regulated by SUMOylation. *Developmental Cell*, *9*(5), 593–603. https://doi.org/10.1016/j.devcel.2005.09.016

Tsujioka, H., Kunieda, T., Katou, Y., Shirahige, K., Fukazawa, T., & Kubo, T. (2017). Interleukin-11 induces and maintains progenitors of different cell lineages during *Xenopus* tadpole tail regeneration. *Nature Communications*, *8*(1),495. https://doi.org/10.1038/s41467-017-00594-5

Viet, J., Reboutier, D., Hardy, S., Lachke, S. A., Paillard, L., & Gautier-Courteille, C. (2020). Modeling ocular lens disease in *Xenopus*. *Developmental Dynamics*, *249*(5), 610–621. https://doi.org/10.1002/dvdy.147

Wagner, T., Wirth, J., Meyer, J., Zabel, B., Held, M., Zimmer, J., Pasantes, J., Bricarelli, F. D., Keutel, J., Hustert, E., Wolf, U., Tommerup, N., Schempp, W., & Scherer, G. (1994). Autosomal sex reversal and campomelic dysplasia are caused by mutations in and around the SRY-related gene *SOX9*. *Cell*, *79*(6), 1111–1120. https://doi.org/10.1016/0092-8674(94)90041-8

Wang, H., Yang, H., Shivalila, C. S., Dawlaty, M. M., Cheng, A. W., Zhang, F., & Jaenisch, R. (2013). One-step generation of mice carrying mutations in multiple genes by CRISPR/Cas-mediated genome engineering. *Cell*, 153(4), 910–918. https://doi.org/10.1016/j.cell.2013.04.025

Wen, R. H., Stanar, P., Tam, B., & Moritz, O. L. (2019). Autophagy in *Xenopus laevis* rod photoreceptors is independently regulated by phototransduction and misfolded RHO ^{P23H}. *Autophagy*, *15*(11), 1970–1989. https://doi.org/10.1080/15548627.2019.1596487

Wright, E., Hargrave, M. R., Christiansen, J., Cooper, L., Kun, J., Evans, T., Gangadharan, U., Greenfield, A., & Koopman, P. (1995). The Sry-related gene *Sox9* is expressed during chondrogenesis in mouse embryos. *Nature Genetics*, *9*(1), 15–20. https://doi.org/10.1038/ng0195-15

Wyatt, B. H., Raymond, T. O., Lansdon, L. A., Darbro, B. W., Murray, J. C., Manak, J. R., & Dickinson, A. J. G. (2021). Using an aquatic model, *Xenopus laevis*, to uncover the role of chromodomain 1 in craniofacial disorders. *Genesis*, *59*(1–2),e23394. https://doi.org/10.1002/dvg.23394

Yasue, A., Kono, H., Habuta, M., Bando, T., Sato, K., Inoue, J., Oyadomari, S., Noji, S., Tanaka, E., & Ohuchi, H. (2017). Relationship between somatic mosaicism of *Pax6* mutation and variable developmental eye abnormalities-an analysis of CRISPR genome-edited mouse embryos. *Scientific Reports*, *7*(1). https://doi.org/10.1038/s41598-017-00088-w

Zeng, L., Kempf, H., Murtaugh, L. C., Sato, M. E., & Lassar, A. B. (2002). Shh establishes an *Nkx3.2/Sox9* autoregulatory loop that is maintained by BMP signals to induce somitic chondrogenesis. *Genes & Development*, *16*(15), 1990–2005. https://doi.org/10.1101/gad.1008002

Zhong, H., Chen, Y., Li, Y., Chen, R., & Mardon, G. (2015). CRISPR-engineered mosaicism rapidly reveals that loss of *Kcnj13* function in mice mimics human disease phenotypes. *Scientific Reports*, *5*(1), 8366. https://doi.org/10.1038/srep08366

Zygar, C. A., Cook, T. Les, & Grainger, R. M. (1998). Gene activation during early stages of lens induction in *Xenopus*. *Development*, *125*(17), 3509–3519. https://doi.org/10.1242/dev.125.17.3509

Figures

(a)

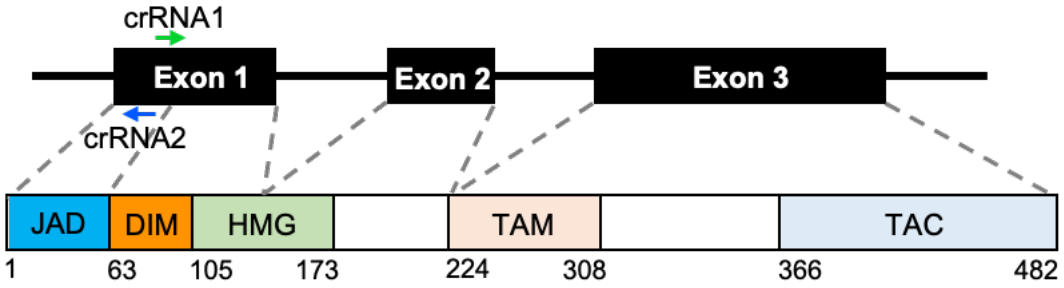

(b)

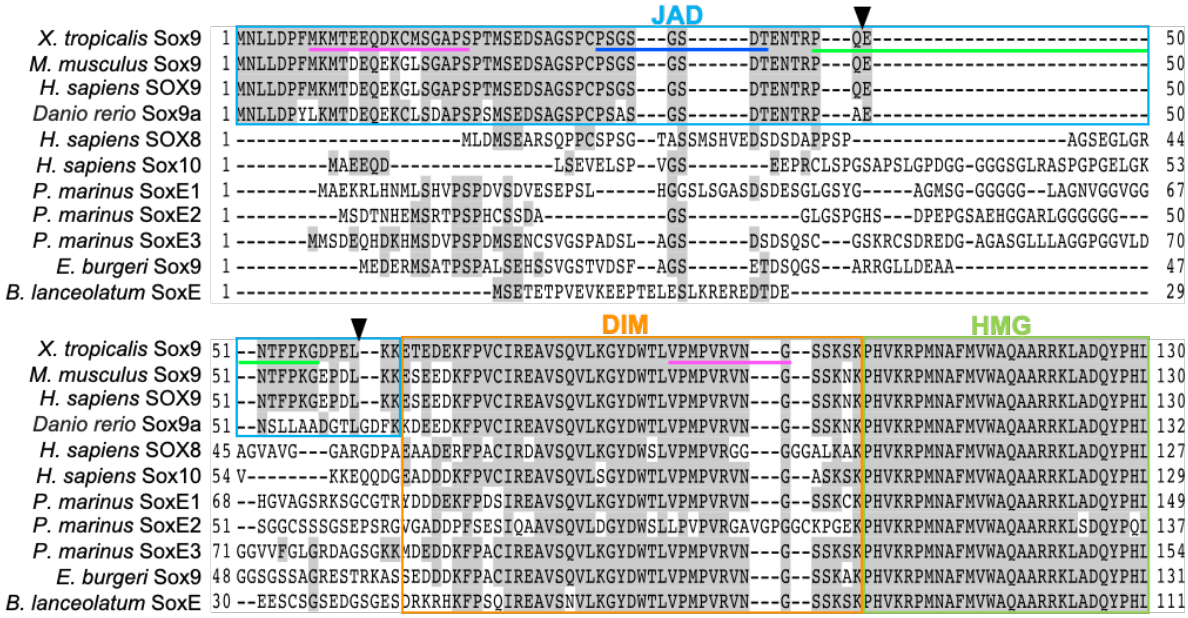

Figure 1: The structure of *X. tropicalis sox9* and design of crRNAs. (a) Schematic illustration of *X. tropicalis sox9* gene and the encoded protein containing the jawed vertebrate-specific amino-terminal domain (JAD), dimerization domain (DIM), DNA-binding HMG domain, transactivating domain in the middle of the protein (TAM), and C terminal transactivation domain (TAC). Amino acid positions are numbered. Green and blue arrows indicate *sox9*-crRNA1 and *sox9*-crRNA2 targeting the exon 1, respectively. (b) An alignment of SoxE family protein sequences (from the amino-terminus to part of the HMG domain) from *X. tropicalis* (Sox9), *Mus musculus* (Sox9), *Homo sapiens* (SOX9), *Danio*

rerio (Sox9a), *H. sapiens* (SOX8), *H. sapiens* (SOX10), *Petromyzon marinus* (SoxE1), *P. marinus* (SoxE2), *P. marinus* (SoxE3), *Eptatretus burgeri* (Sox9), and *Branchiostoma lanceolatum* (SoxE). Amino acid sequences identical to those of *X. tropicalis* Sox9 are shaded in gray in the SoxE proteins of other species. The JAD, DIM, and HMG domains are boxed in cyan, orange, and light green, respectively. Magenta lines indicate amino acids encoded by target nucleotide sequences of a pair of PCR primers used to prepare amplicons for genotyping crispants. Green and blue lines indicate amino acids encoded by target nucleotide sequences of crRNA1 and crRNA2, respectively. Black triangles indicate the range of in-frame deletions identified in Category 1/2 tadpoles (Figure 5a). Accession numbers for the sequences used in the alignment: *X. tropicalis* (Sox9: AAT72000.1); *M. musculus* (Sox9: AAH23953.1); *H. sapiens* (Sox8: NP_055402.2, Sox9: NP_000337.1, Sox10: NP_008872.1); *D. rerio* (Sox9a: NP_571718.1); *P. marinus* (SoxE1: AAW34332.1, SoxE2: ABC58684.1, SoxE3: ABC58685.1); *E. burgeri* (Sox9: BAG11536.1); *B. lanceolatum* (SoxE: CAH1273350.1).

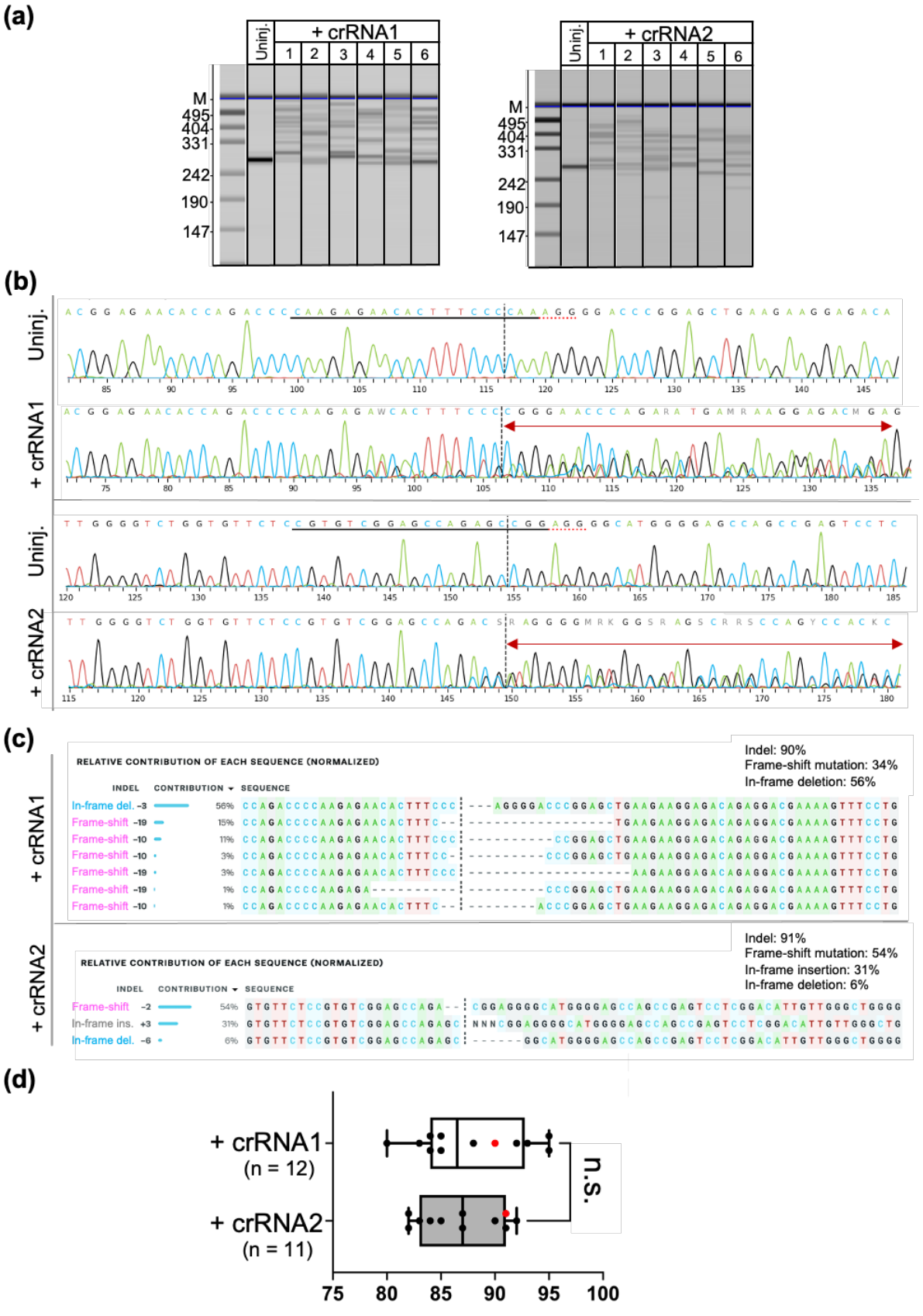
(a)
Uninj.
+ crRNA1
1 2 3 4 5 6
M
495
404
331
242
190
147
Uninj.
+ crRNA2
1 2 3 4 5 6
M
495
404
331
242
190
147
(b)
Uninj.
+ crRNA1
Uninj.
+ crRNA2
(c)
+ crRNA1
RELATIVE CONTRIBUTION OF EACH SEQUENCE (NORMALIZED)
INDEL CONTRIBUTION SEQUENCE
In-frame del. -3 56%
Frame-shift -19 15%
Frame-shift -10 11%
Frame-shift -10 3%
Frame-shift -19 3%
Frame-shift -19 1%
Frame-shift -10 1%
Indel: 90%
Frame-shift mutation: 34%
In-frame deletion: 56%
+ crRNA2
RELATIVE CONTRIBUTION OF EACH SEQUENCE (NORMALIZED)
INDEL CONTRIBUTION SEQUENCE
Frame-shift -2 54%
In-frame ins. +3 31%
In-frame del. -6 6%
Indel: 91%
Frame-shift mutation: 54%
In-frame insertion: 31%
In-frame deletion: 6%
(d)
+ crRNA1
(n = 12)
+ crRNA2
(n = 11)
n.s.
75 80 85 90 95 100

Figure 2: Analysis of genome editing efficiency by *sox9*-crRNA1 and sox9-crRNA2. (a) HMA of target genomic region amplicons prepared from tadpoles injected with *sox9*-crRNA1 or *sox9*-crRNA2. Gel images were generated from electropherograms of the amplicons. The leftmost lane indicates molecular markers. "M" at the left of the maker lane indicates the position of internal control bands for comparing mobilities of DNA fragments among samples, and numbers indicate the marker lengths (bp). Lanes labeled "Uninj." show gel electrophoresis patterns of amplicons prepared from uninjected tadpoles, and lanes labeled from 1 to 6 show those of amplicons prepared from *sox9*-crRNA1- or *sox9*-crRNA2-injected tadpoles. (b) Representative Sanger chromatograms of the target region amplicons from uninjected tadpoles or tadpoles injected with *sox9*-crRNA1 or *sox9*-crRNA2. Horizontal black lines and red dotted lines indicate target sequences of the crRNAs and PAM sequences, respectively. Black dotted lines and red double-sided arrows indicate cleavage sites and the downstream mutated regions predicted by the ICE analysis, respectively. Note that nucleotide deletions occurred in part of the cells not only in downstream regions of the cleavage site but also in the short upstream regions, as shown in previous CRISPR/Cas9 genome editing studies (Tanouchi et al., 2022) (Sieliwonczyk et al., 2023). (c) ICE analysis outputs of the Sanger chromatograms shown in (b). Insertion and deletion bases in allelic series of mutations of each tadpole injected with *sox9*-crRNA1 or *sox9*-crRNA2 are shown as "INDEL" with "-" and "+" that indicate deletion and insertion, respectively. A percentage of each mutated allele in the total alleles of an individual tadpole is shown as a "contribution." Black dotted lines indicate the cleavage sites predicted by the ICE analysis. Nucleotides identical to those of uninjected tadpoles are shown as A, G, C, or T, and inserted nucleotides are shown as N in the alignments. The ICE analysis tool does not align sequences downstream of inserted sequences. Frame-shift: frame-shift mutation. In-frame del.: in-frame deletion. In-frame ins.: in-frame insertion. (d) A box-and-whisker plot showing indel percentages calculated by the ICE analysis for tadpoles injected with *sox9*-crRNA1 or *sox9*-crRNA2 as dots. In each sample group, horizontal lines indicate the minimum, first quartile, median (Med.), third quartile, and maximum values, respectively, from bottom to top. The unpaired t-test indicated no significant difference (n.s.) in the indel ratios between the *sox9*-crRNA1- and *sox9*-crRNA2-injected tadpoles. Samples shown as representative cases in (b) and (c) are marked red in the graph.

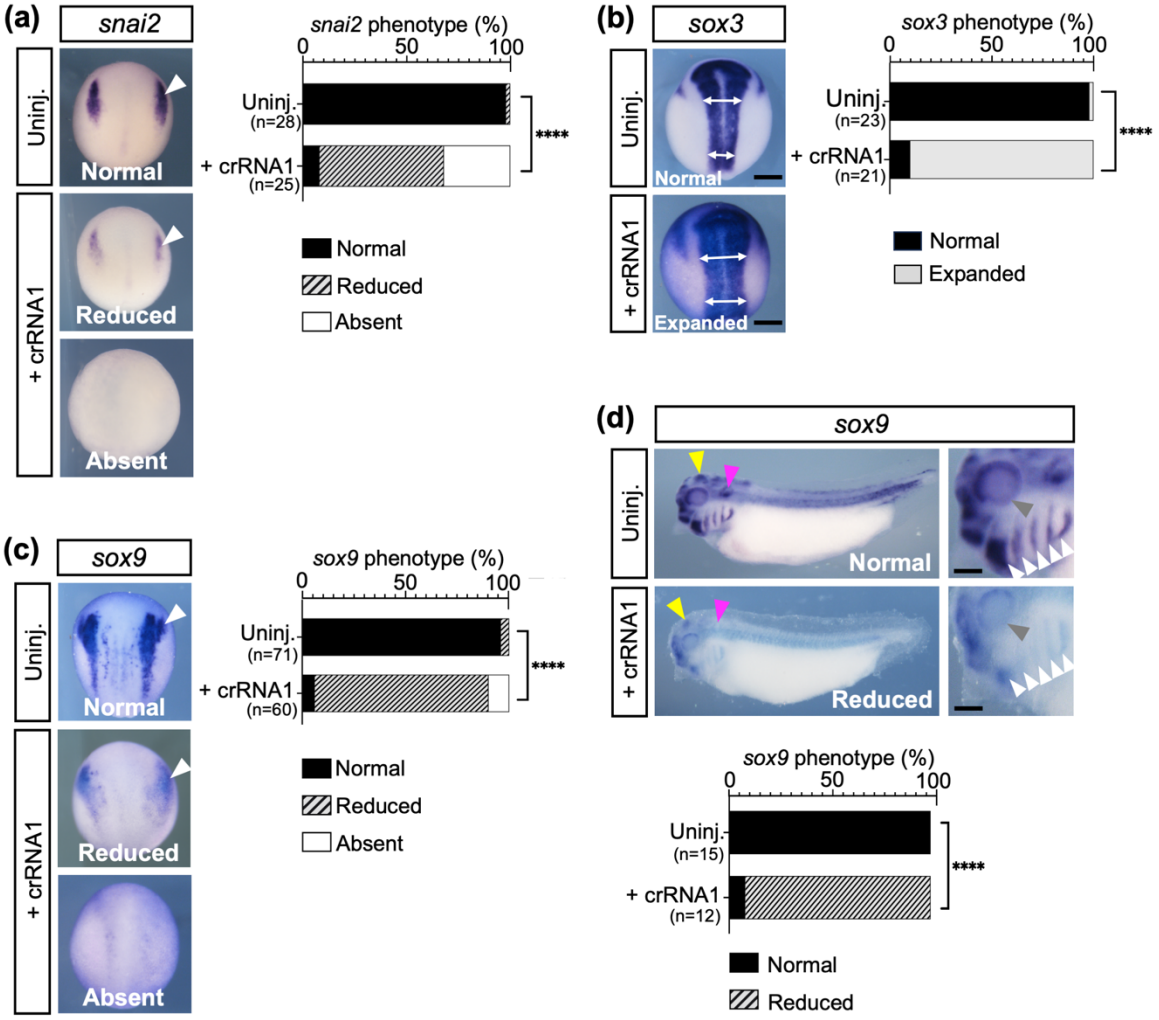
(a)
snai2
Uninj.
+ crRNA1
Normal
Reduced
Absent
snai2 phenotype (%)
0
50
100
Uninj.
(n=28)
+ crRNA1
(n=25)
****
Normal
Reduced
Absent
(b)
sox3
Uninj.
+ crRNA1
Normal
Expanded
sox3 phenotype (%)
0
50
100
Uninj.
(n=23)
+ crRNA1
(n=21)
****
Normal
Expanded
(c)
sox9
Uninj.
+ crRNA1
Normal
Reduced
Absent
sox9 phenotype (%)
0
50
100
Uninj.
(n=71)
+ crRNA1
(n=60)
****
Normal
Reduced
Absent
(d)
sox9
Uninj.
+ crRNA1
Normal
Reduced
sox9 phenotype (%)
0
50
100
Uninj.
(n=15)
+ crRNA1
(n=12)
****
Normal
Reduced

Figure 3

Figure 3: Expression analysis of neural crest, neural plate marker genes, and *sox9* in *sox9* crispant embryos. (a) Dorsal views of uninjected and *sox9*-crRNA1-injected neurula embryos (stages 15–16) hybridized with *snai2* probe. White triangles indicate expression signals of *snai2* in the neural crest cells. Expression patterns were classified into "normal," "reduced," or "absent," and scoring results were summarized in a bar graph. (b) Dorsal views of uninjected and *sox9*-crRNA1-injected neurula embryos (stages 15–16) hybridized with *sox3* probe. White double-sided arrows indicate the widths of the *sox3*-expressing neural plate. Expression patterns were classified into "normal" and "expanded," and scoring results were summarized in a bar graph. (c) Dorsal views of uninjected and *sox9*-crRNA1-injected neurula embryos (stages 15–16) hybridized with *sox9* probe. White triangles indicate expression signals of *sox9* in the neural crest cells. Expression patterns were scored and summarized in a bar graph as in (a). (d) Lateral views of uninjected and *sox9*-crRNA1-injected tailbud embryos (stages 34/35) hybridized with *sox9* probe. White, magenta, gray, and yellow triangles indicate pharyngeal arches, otic vesicles, eye, and brain, respectively. Expression patterns were classified into "normal" and "reduced," and scoring results were summarized in a bar graph. In all cases, the data were statistically analyzed using the Fisher's exact test (****$p < 0.0001$). The number of analyzed embryos is shown in the graph. Scale bars indicate 50 μm. Representative embryos are shown for each probe.

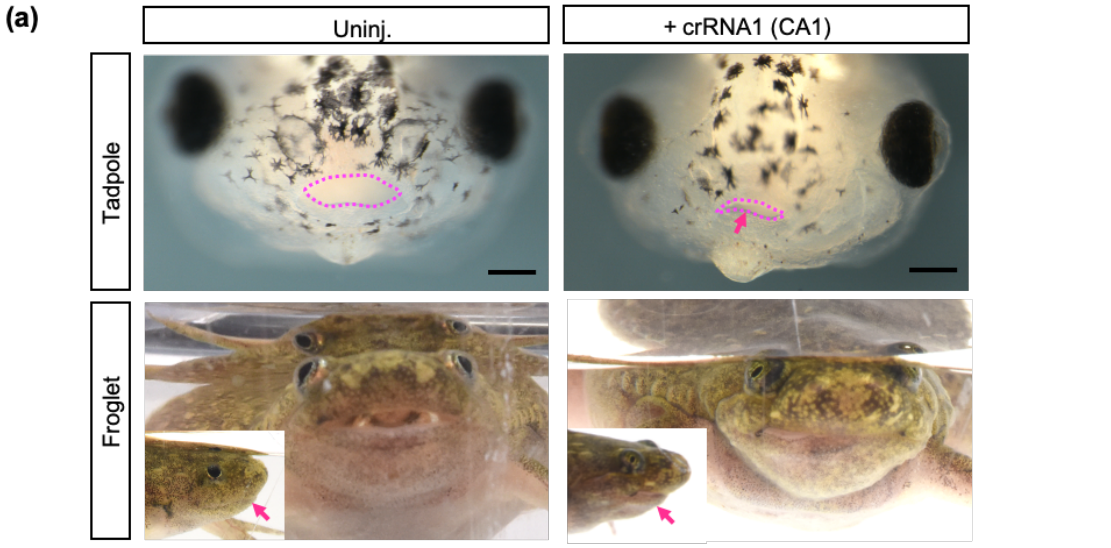
(a)
Uninj.
+ crRNA1 (CA1)
Tadpole
Froglet

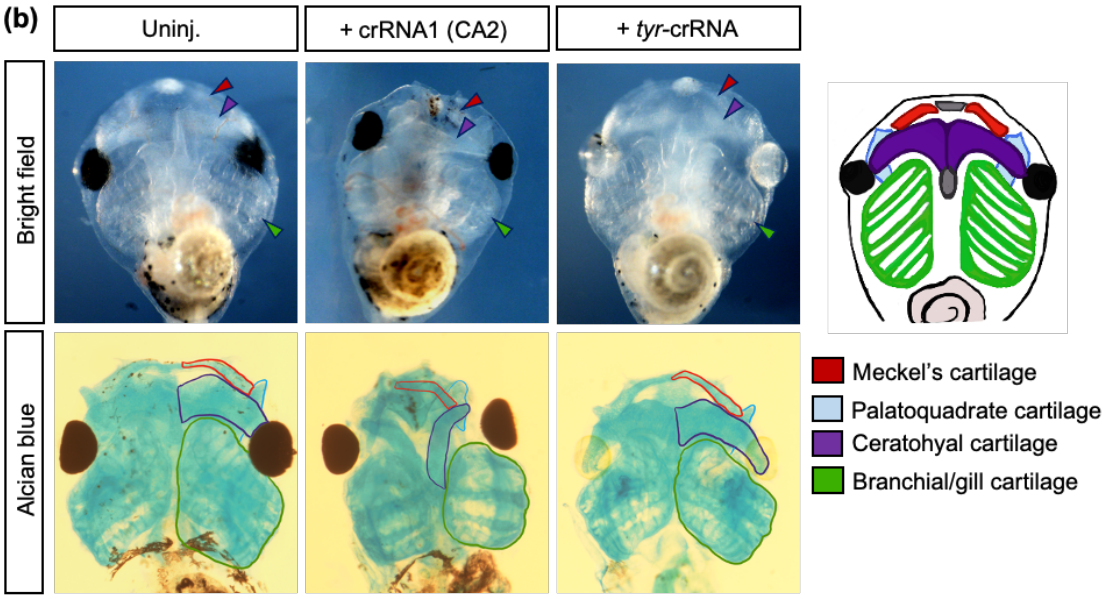
(b)
Uninj.
+ crRNA1 (CA2)
+ tyr-crRNA
Bright field
Alcian blue
Meckel's cartilage
Palatoquadrate cartilage
Ceratohyal cartilage
Branchial/gill cartilage

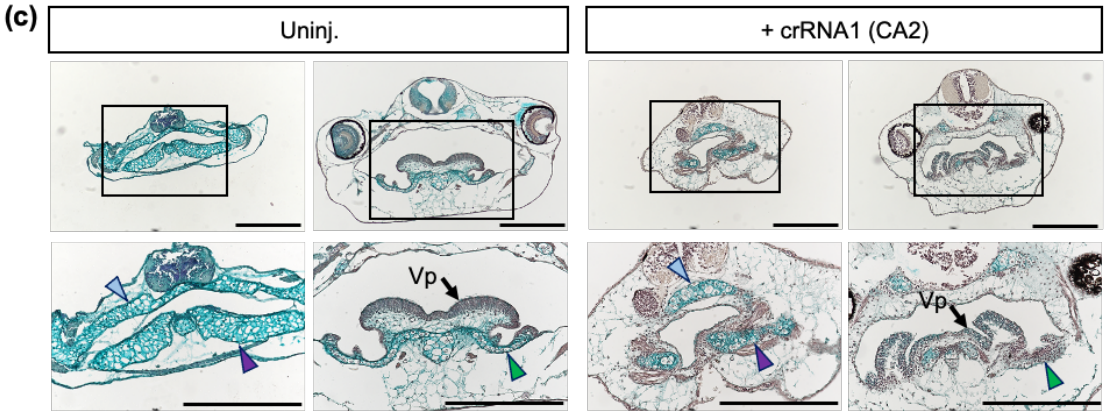
(c)
Uninj.
+ crRNA1 (CA2)
Vp
Vp

Figure 4: Syndromic defects in *sox9* crispant tadpoles (a-c). a) Frontal views of an uninjected tadpole and a representative *sox9*-crRNA1-injected tadpole with the Category 1 (CA1) phenotype (refer (h) for the phenotypic classification; Upper panel: tadpole stage and lower panel: froglet). Magenta dotted lines delineate their mouth openings, and a magenta arrow indicates jaw deformity in the injected tadpole. The lower haw deformity at froglet stage of an uninjected and representative sox9-crRNA1 injected is shown in lower panel. In lower panel, the lower jaw defect at froglet stage is indicated with pink arrow.(b) Ventral views of an uninjected tadpole, a representative *sox9*-crRNA1-injected tadpole exhibiting jaw, gill, and inner ear defects without apparent defects in other organs (Category 2 (CA2)), and a representative *tyr*-crRNA-injected tadpole with the albino phenotype, along with a schematic ventral view of the craniofacial cartilages of a tadpole. The upper panels are bright-field images, with red, purple, and green triangles indicating Meckel's, ceratohyal, and branchial cartilages, respectively. Palatoquadrate cartilages are unclear in the bright-field images. The lower panels are images of Alcian blue-stained tadpoles, where blue, red, purple, and green lines delineate palatoquadrate, Meckel's, ceratohyal, and branchial cartilages, respectively, in the left side of the bodies. (c) Transverse sections of an uninjected tadpole and a representative *sox9*-crRNA1-injected tadpole with the CA2 phenotype. In both image sets of the uninjected and injected tadpoles, the left panels show cross-sections through anterior to the eyes, and the right panels show cross-sections through the eyes. Lower panels are high-magnification images of the area enclosed by the squares in upper panels. Vp: velar plate. Colored triangles indicate the cartilages as in (b). Chondrocytes were stained in turquoise with Alcian blue.

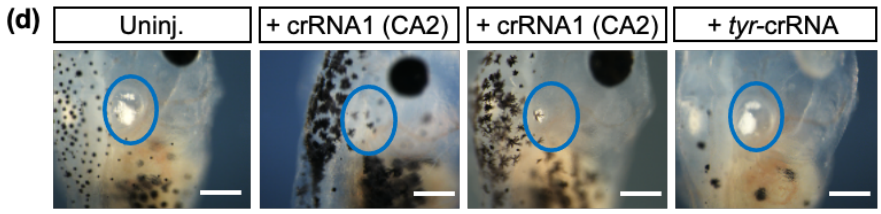

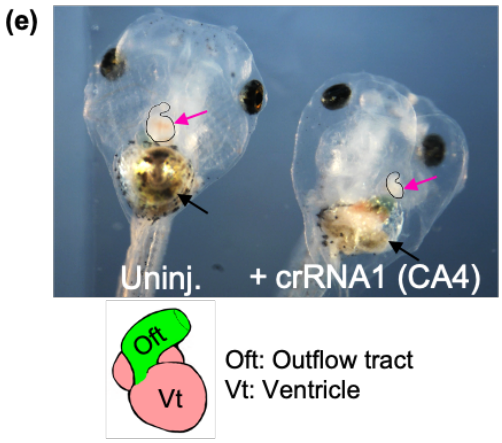

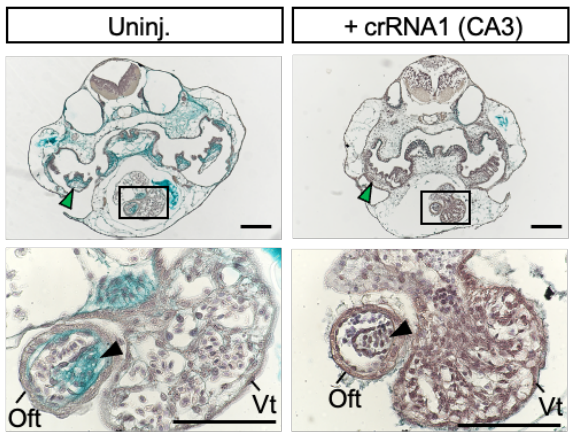

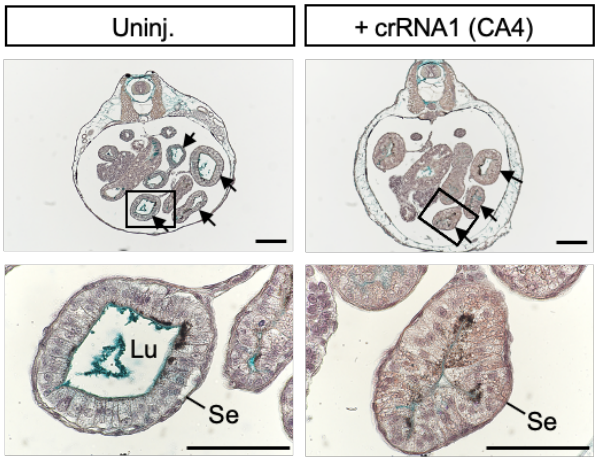

(h) Phenotype categories

	J/Gi	IE	H	Gu	B
CA1	+	-	-	-	-
CA2	+	+	-	-	-
CA3	+	+	+	-	-
CA4	+	+	+	+	-
CA5	+/-	+/-	+/-	+/-	+

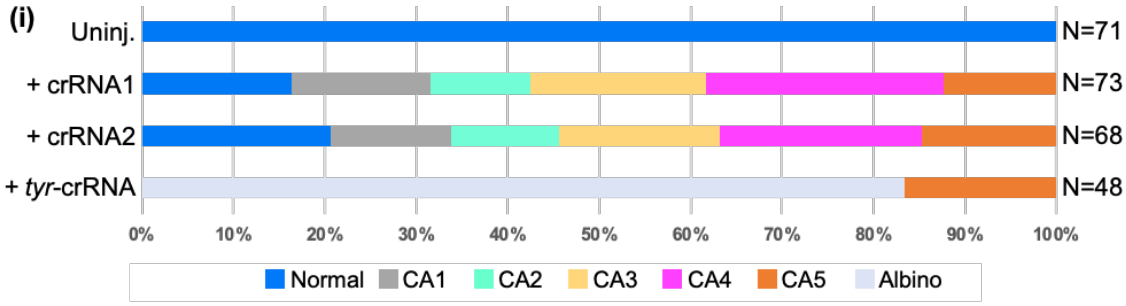

Figure 4: Syndromic defects in *sox9* crispant tadpoles (d-i). (d) Dorsolateral views of the inner ears of an uninjected tadpole and representative *sox9*-crRNA1-injected tadpoles with the CA2 phenotype, and *tyr*-crRNA-injected tadpole. Blue circles indicate otoliths formed in the ear vesicles. (e) Ventral view of an uninjected tadpole and a representative *sox9*-crRNA1-injected tadpole exhibiting heart and gut defects in addition to the jaw, gill, and inner ear defects (Category 4 (CA4)), and a schematic diagram of a tadpole heart. Magenta and black arrows indicate the heart and gut, respectively. Black lines delineate the heart shape in both tadpoles. Oft: outflow tract, Vt: ventricle. (f) Transverse sections through the hearts of an uninjected tadpole and a representative *sox9*-crRNA1-injected tadpole exhibiting heart defects in addition to the jaw, gill, and inner ear defects (Category 3 (CA3)). Lower panels are high-magnification images of the area enclosed by the squares in upper panels. Green and black triangles indicate the branchial cartilages and the lumen of outflow tracts, respectively. Note that Alcian blue-stained chondrocytes in the branchial cartilages and cardiac jelly in the outflow tract lumen were severely reduced in the *sox9*-crRNA1-injected tadpole compared to the uninjected tadpole. (g) Transverse sections through the intestines of an uninjected tadpole and a representative *sox9*-crRNA1-injected tadpole with the CA4 phenotype. Lower panels are high-magnification images of the area enclosed by the squares in upper panels. Black arrows indicate the intestines. The columnar epithelium facing the lumen (Lu) is visible and externally surrounded by the serosa (Se). The columnar epithelium was thickened, and the lumen was severely reduced in the *sox9*-crRNA1-injected tadpole compared to the uninjected tadpole. Scale bars indicate 100 μm in (a), (c), (d), (f), and (g). (h) Phenotypic classification of tadpoles injected with *sox9*-crRNA1 or *sox9*-crRNA2**.** The defective phenotypes observed were classified into six categories, CA1 (jaw and gill defects only), CA2 (jaw, gill, and inner ear defects only), CA3 (jaw, gill, inner ear, and heart defects only), CA4 (jaw, gill, inner ear, heart, and gut defects), and CA5 (body bending with or without other defects). The "J/Gi," "IE," "H," "Gu," and "B" indicate jaw and gill, inner ear, heart, gut, and body bending defects, respectively. The "+" and "-" indicate the presence and absence of these defects in each phenotypic category, respectively. (i) Macroscopic scoring results of phenotypes classified into normal, CA 1 to CA5, and albino in uninjected, *sox9*-crRNA1-injected, *sox9*-crRNA2-injected, and *tyr*-crRNA-injected tadpoles at stages 42-45. Tadpoles exhibiting partial or complete pigment loss

without any other apparent defects were scored as albinos in the group of *tyr*-crRNA-injected individuals. The number of analyzed embryos is shown in each graph.

(a)

crRNA1

		INDEL	(%)	49	50	51	52	53	54	55	56	57	58	59	60	61	
		WT		Q	E	N	T	F	P	K	G	D	P	E	L	K	
CA1	In-frame del.	-9bp	29	Q	E	N	T	F	P	-	-	-	P	E	L	K	
		-3bp	26	Q	E	N	T	F	P	-	G	D	P	E	L	K	
		-18bp	10	Q	E	N	T	F	P	-	-	-	-	-	-	K	
		-18bp	6	Q	-	-	-	-	-	-	G	D	P	E	L	K	
		-18bp	6	Q	E	N	T	F	-	-	-	-	-	-	L	K	
	Frame-shift	-10bp	6	Q	E	N	T	F	P	R	S	X					
		-10bp	3	Q	E	N	T	G	T	R	S	X					
		-10bp	3	Q	E	N	T	F	T	R	S	X					
		-11bp	2	Q	E	N	T	F	P	G	A	E	E	G	D	R	*
		-5bp	1	Q	E	N	T	F	P	G	P	G	A	E	E	G	*
CA4	Frame-shift	-11bp	20	Q	E	N	T	F	P	G	A	E	E	G	D	R	
		-7bp	18	Q	E	N	T	F	P	T	R	S	X				
	In-frame del.	-12bp	17	Q	E	N	T	F	P	-	-	-	-	E	L	K	
	Frame-shift	-4bp	15	Q	E	N	T	F	P	G	T	R	S	X			
		-5bp	14	Q	E	N	T	F	P	G	P	G	A	E	E	G	*
		-5bp	6	Q	E	N	T	F	R	G	P	G	A	E	E	G	*
		-7bp	1	Q	E	N	T	F	R	T	R	S	X				

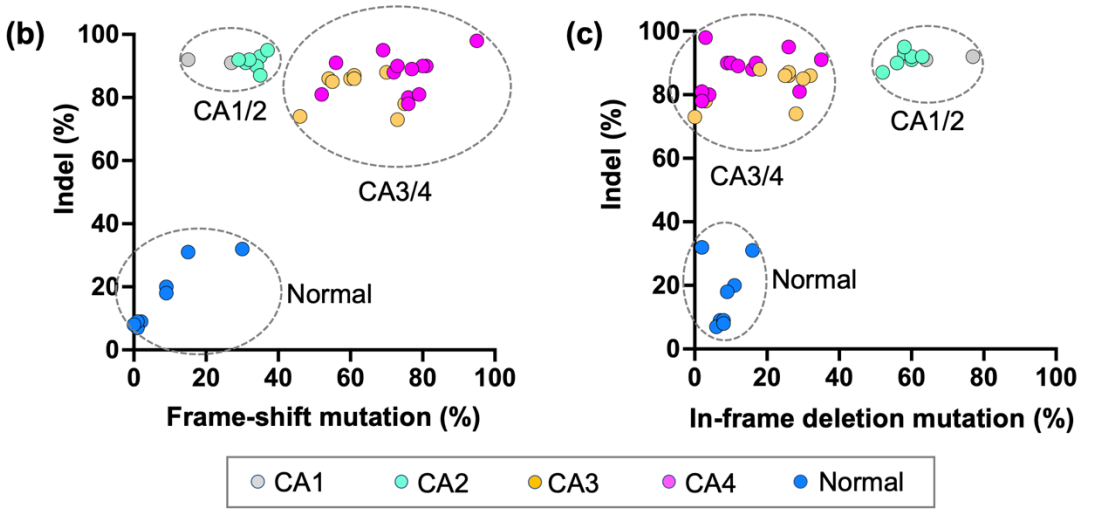

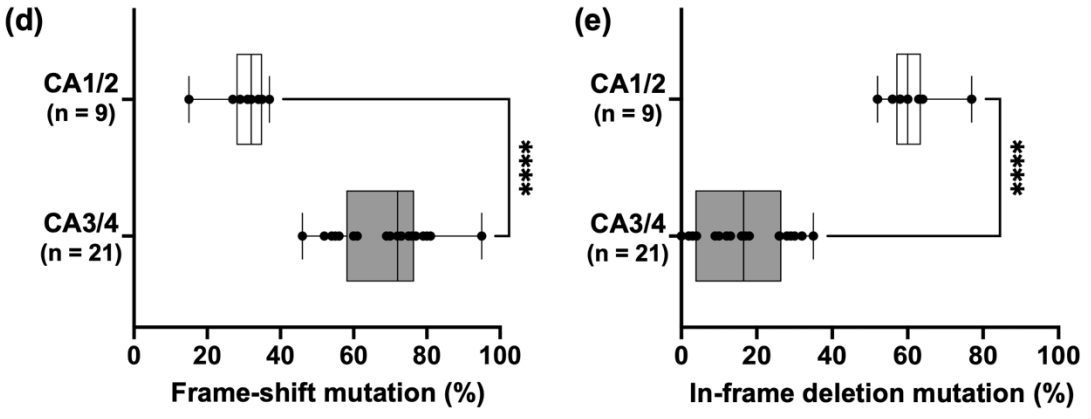

Figure 5: Phenotype-genotype correlation in *sox9* crispants. (a) Amino acid sequences encoded by the mosaic *sox9* alleles of representative CA1 and CA4 tadpoles. The sequence deduced from each allele is aligned with the corresponding sequence of wild-type Sox9. Amino acids identical to those of the wild type were shaded in gray. Amino acids deleted in the in-frame deletion alleles are indicated by "-". Amino acids deleted in the frame-shift alleles are indicated by either "X" (stop codon) or empty spaces. Asterisks indicate frame-shift alleles whose stop codons locate downstream of the aligned regions. A percentage of each mutant allele in the total alleles of an individual tadpole is shown. A green line indicates amino acids encoded by the target nucleotide sequence of crRNA1. Cyan and magenta triangles indicate the ranges of in-frame deletions and frame-shift starting points identified in all the tadpoles used for the phenotype-genotype correlation analysis (not just these representative tadpoles), respectively. A white triangle indicates a potential SUMOylation site (Taylor & LaBonne, 2005). The ICE analysis outputs used for generating these amino acid sequence alignments are shown in Figure S2. (b) Relationships between indel ratios and frame-shift mutation (insertion and deletion) ratios in mosaic alleles of *sox9*-crRNA1-injected tadpoles. (c) Relationships between indel ratios and in-frame deletion (without any insertions) ratios in mosaic alleles of *sox9*-crRNA1-injected tadpoles. Data for Category 1 - 4 (CA1 - CA4) tadpoles and the injected tadpoles with normal morphology are plotted with the color codes shown in the bottom. Dotted circles indicate groups of the CA1 and CA2 tadpoles, CA3 and CA4 tadpoles, and tadpoles with normal morphology. (c) A box-and-whisker plot shows frame-shift mutation ratios in mosaic alleles of CA1 and CA2 tadpoles (CA1/2) and those of CA3 and CA4 tadpoles (CA3/4) as dots. (d) A box-and-whisker plot shows in-frame deletion ratios in mosaic alleles of CA1 and CA2 tadpoles (CA1/2) and those of CA3 and CA4 tadpoles (CA3/4) as dots. In each sample group, vertical lines indicate the minimum, first quartile, median (Med.), third quartile, and maximum values, respectively, from left to right. The data were statistically analyzed using the unpaired t-test (****$p < 0.0001$).

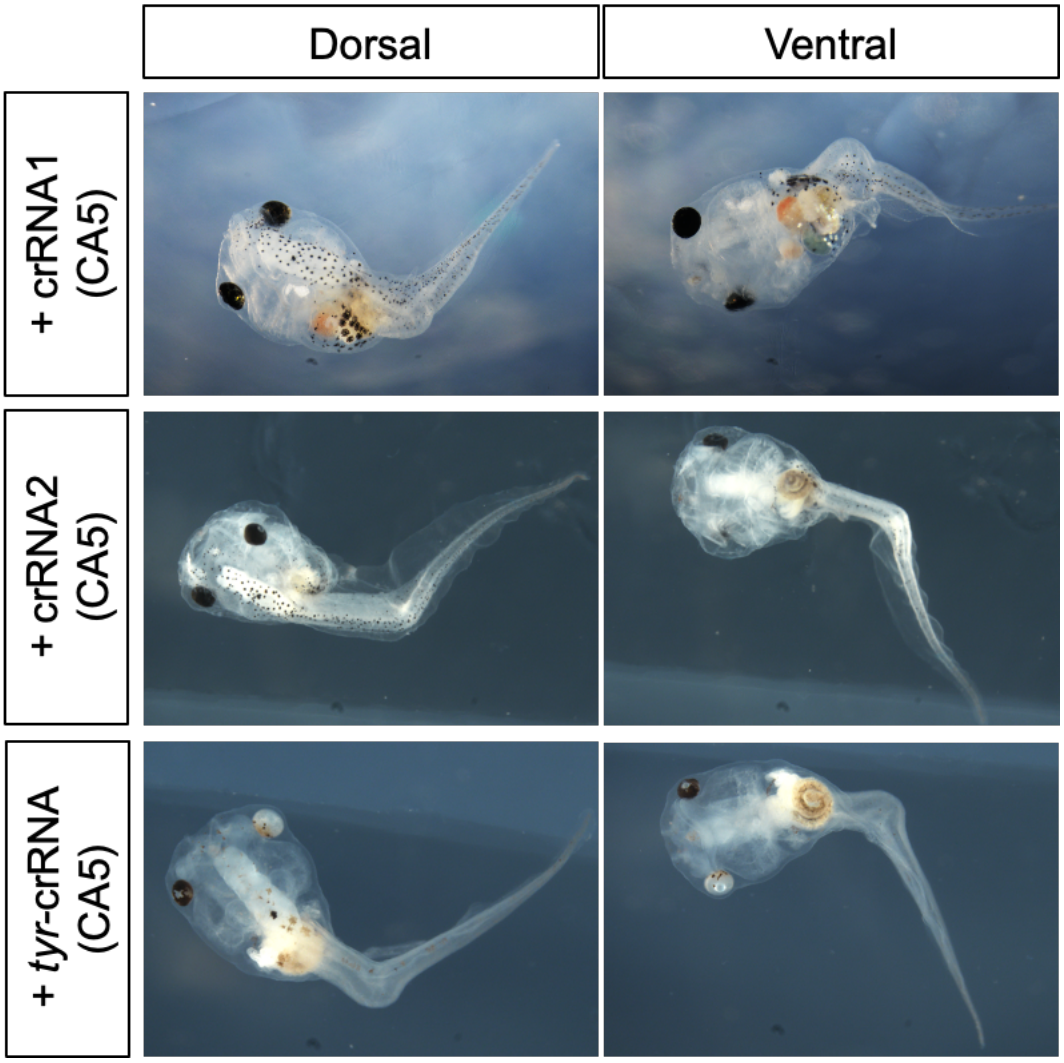

Supplementary Figure S1. Representative crispant tadpoles exhibiting the Category 5 phenotype. Dorsal and ventral views of tadpoles injected with *sox9*-crRNA1 (upper panels), *sox9*-crRNA2 (middle panels), or *tyr*-crRNA (bottom panels). Representative cases exhibiting Category 5 phenotype are shown. Triangles indicate bent parts of their bodies. Note that part of the Category 5 tadpoles injected with *sox9*-crRNA1 or *sox9*-crRNA2 exhibited cranial defects, whereas the Category 5 tadpoles injected with *tyr*-crRNA exhibited a melanin loss phenotype.

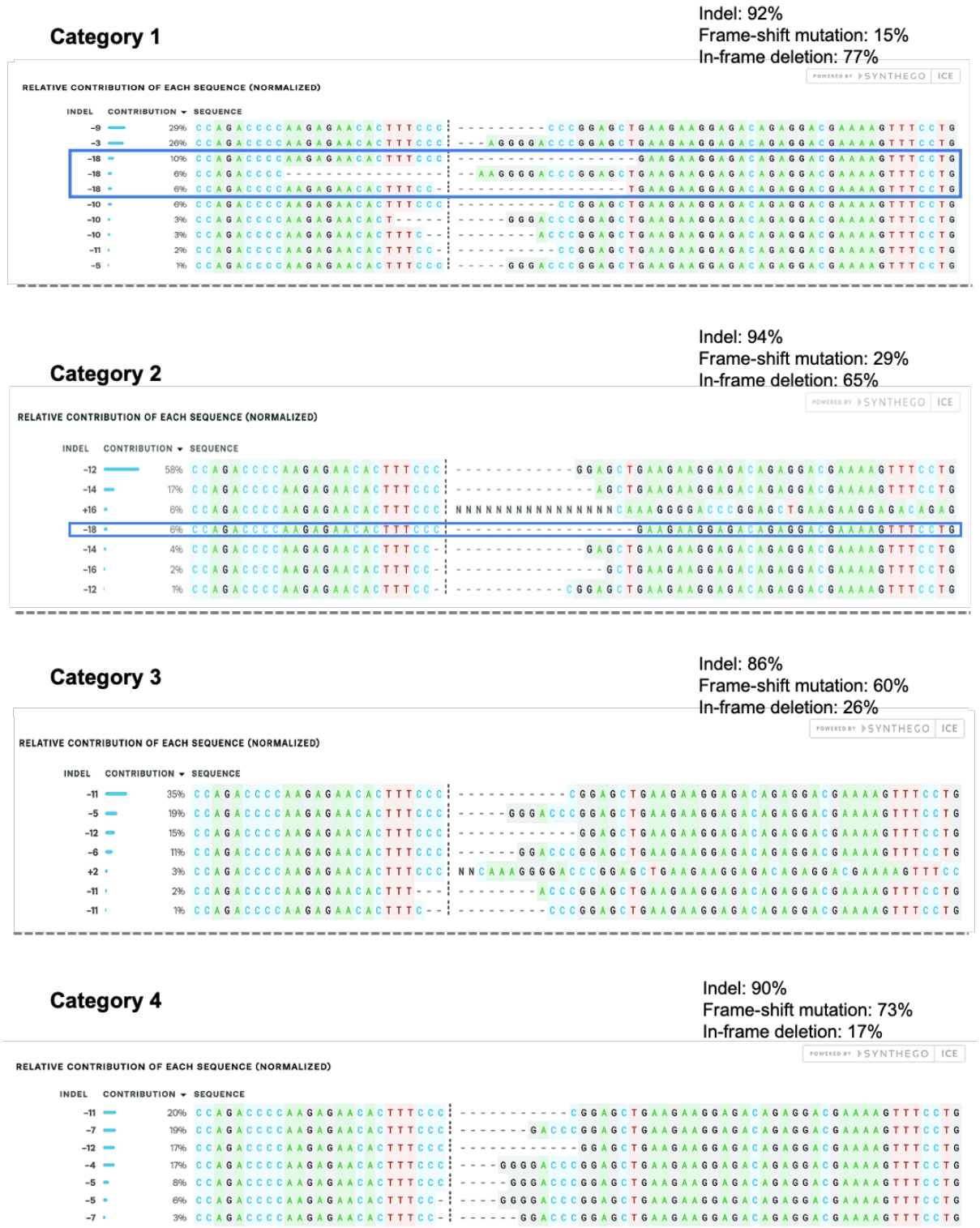

Supplementary Figure S2. Representative outputs of ICE analysis in *sox9* crispants with Category 1 - 4 phenotype. Insertion and deletion bases in allelic series of mutations of each tadpole are shown as "INDEL" with "-" and "+" that indicate deletion and insertion, respectively. A percentage of each mutated allele in the total alleles of an individual tadpole is shown as a

"contribution." Indel, frame-shift mutation (deletion and insertion), and in-frame deletion mutation ratios were calculated with the percentages of these alleles. Black dotted lines indicate the cleavage sites predicted by the ICE analysis. Nucleotide sequences identical to those of uninjected tadpoles and insertion sequences are indicated by "A, G, C, T" and "N," respectively, in the alignments. Blue boxes indicate the maximum in-frame deletions identified in the Category 1/2 tadpoles. The top and bottom data were used to generate amino acid sequence alignments shown in Figure 5a.

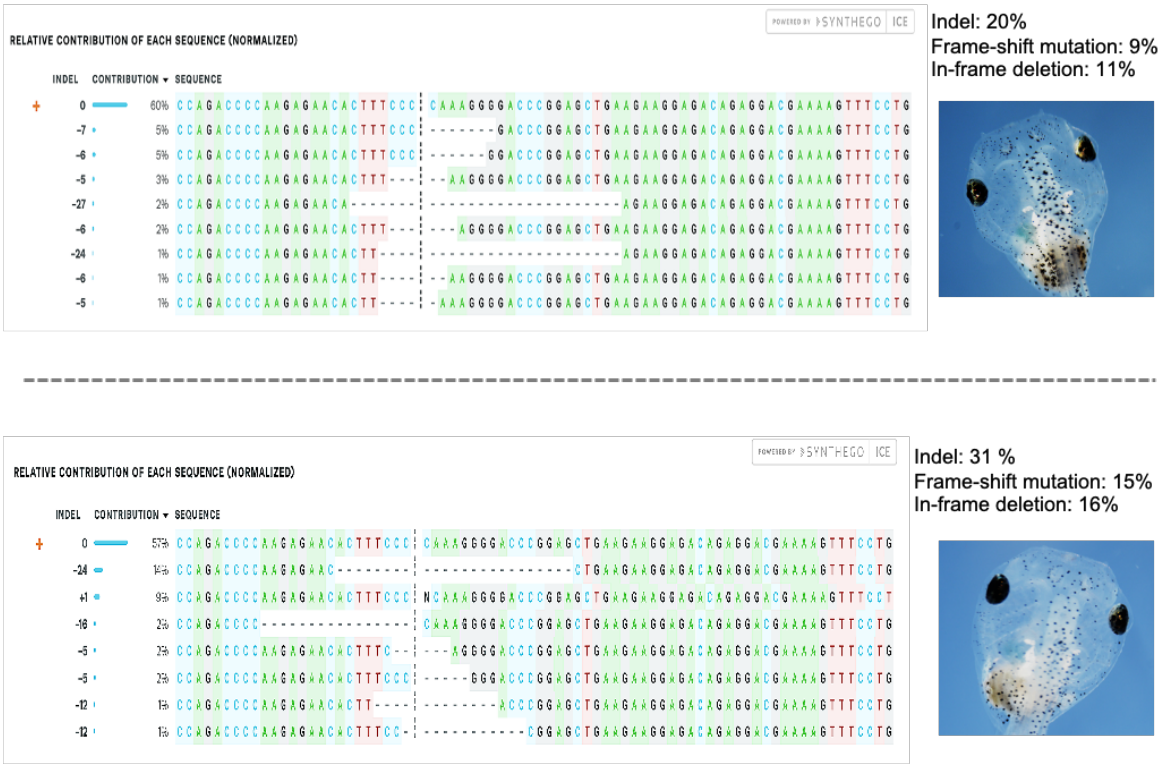

Supplementary Figure S3. Representative outputs of ICE analysis in *sox9* crispants with normal morphology. Two representative data are shown with dorsal views of the tadpoles. Indel, frame-shift mutation (deletion and insertion), and in-frame deletion mutation ratios were calculated as in Figure S2.

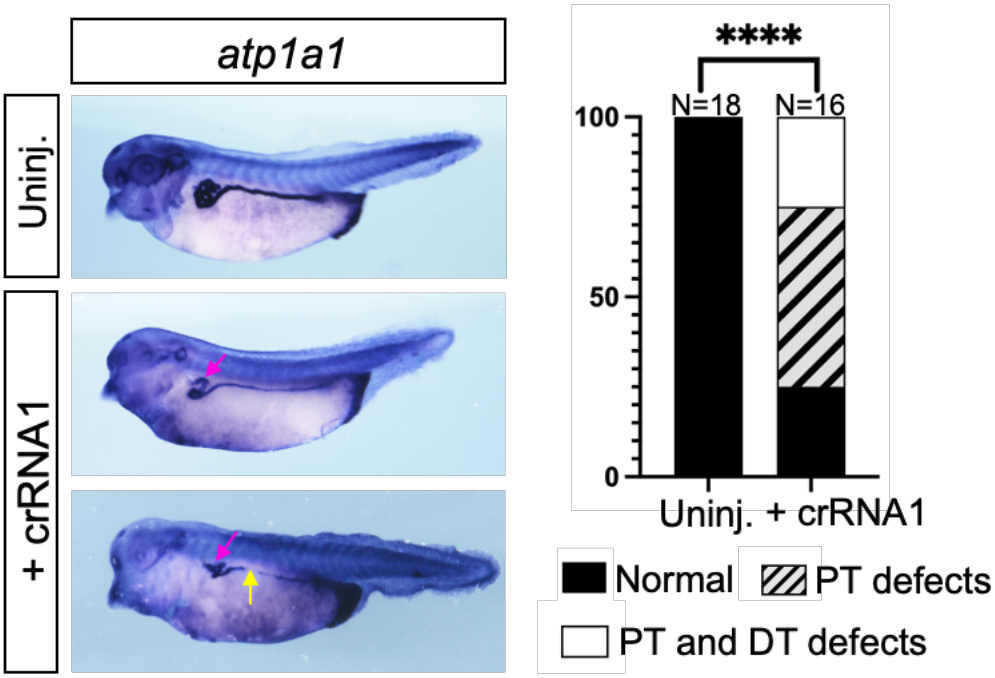

Supplementary Figure S4. Pronephric defects in *sox9* crispants. Lateral views of uninjected and *sox9*-crRNA1-injected tailbud embryos (stages 35/36) hybridized with *atp1a1* probe, with bar graphs summarizing scoring results of its expression patterns. Magenta and yellow arrows indicate proximal and distal tubule defects, respectively. The defects detected by *atp1a1* expression in the crispants were classified into "normal," "proximal tubule (PT) defect," and "proximal tubule (PT) and distal tubule (DT) defects" for the scoring. The data were statistically analyzed using the chi-square test (****$p < 0.0001$).

Acknowledgments

First, I express my sincere gratitude to my supervisor, Professor Dr. Hajime Ogino, for giving me the opportunity to continue my PhD under his supervision. Over the last few years, his immense support, patience, and motivation have helped me gain confidence in becoming a better research scholar. Despite his busy schedule, he was always available to answer my questions and provide feedback. His mentorship has profoundly impacted my life in a way that I cannot even describe in words, and I am genuinely grateful to him. Besides my supervisor, I am also thankful to Associate Professor Dr. Takeshi Igawa and Assistant Professor Dr. Makoto Suzuki for their insightful suggestions. I was able to achieve my research goals thanks to their continuous guidance. I also received valuable advice and constructive feedback from Professor Dr. Takuya Imamura and Professor Dr. Toshinori Hayashi, which helped me improve my doctoral dissertation. Additionally, I am grateful to Assistant Professor Dr. Ichiro Tazawa for providing me with training and chemicals involved in the histological studies of my research. I want to thank all the members of Ogino Lab and the Amphibian Research Center for their encouragement and understanding, which greatly smoothed the path of my PhD journey in this wonderful land of the rising sun.

Finally, I would like to thank my family, especially my father, for protecting my sanity through his unconditional love and mental support throughout the years. Coming from a conservative family background, I had to make many sacrifices to pursue my PhD, but I hope that my story will encourage other female researchers in my country to follow their dreams and contribute more to science.